# Linking the Surface and Subsurface in River Deltas - Part 1: Relating Surface and Subsurface Geometries

**Jayaram Hariharan[1], Zhongyuan Xu[2], Holly A. Michael[2,3], Chris Paola[4], Elisabeth Steel[5], Paola Passalacqua[1]**

[1]Department of Civil, Architectural and Environmental Engineering and Center for Water and the Environment, University of Texas at Austin, Austin, Texas, USA
[2]Department of Earth Sciences, University of Delaware, Newark, Delaware, USA
[3]Department of Civil and Environmental Engineering, University of Delaware, Newark, Delaware, USA
[4]Department of Earth and Environmental Sciences, University of Minnesota, Minneapolis, Minnesota, USA
[5]Department of Geologic Science and Geologic Engineering, Queen's University, Kingston, Ontario, Canada

**Key Points:**

- We investigate whether delta surface channel network metrics can inform predictions of subsurface properties
- Higher surface wetted fraction values and more variable shoreline roughness values are associated with increased connectivity in the subsurface
- The Kullback-Leibler divergence identifies shoreline roughness, wetted fraction, 2-D connectivity, and 2-D percolated path ratio as the most unique metrics

Corresponding author: P. Passalacqua, `paola@austin.utexas.edu`

**Abstract**
River deltas are densely populated regions of the world with vulnerable groundwater reserves. Contamination of these groundwater aquifers via saline water intrusion and pollutant transport is a growing threat due to both anthropogenic and climate changes. The arrangement and composition of subsurface sediment is known to have a significant impact on aquifer contamination; however, developing accurate depictions of the subsurface is challenging. In this work, we explore the relationship between surface and subsurface properties and identify the metrics most sensitive to different forcing conditions. To do so, we simulate river delta evolution with the rule-based numerical model, DeltaRCM, and test the influence of input sand fraction (ISF) and steady sea level rise (SLR) on delta evolution. From the model outputs we measure a variety of surface and subsurface metrics chosen based on their applicability to imagery and modeling results. The Kullback-Leibler (KL) divergence is then used to quantitatively gauge which metrics are most indicative of the imposed forcings. Both qualitative observations and the KL divergence analysis suggest that estimates of subsurface connectivity can be constrained using surface information. In particular, more variable shoreline roughness values and higher surface wetted fraction values correspond to increased subsurface connectivity. These findings complement traditional methods of estimating subsurface structure in river-dominated delta systems and represent a step towards the identification of a direct link between surface observations and subsurface form.

## Plain Language Summary

River deltas are home to over half a billion people facing increasing risks due to a variety of natural and human-induced factors. With rising sea levels, one of the expected threats to public health is the contamination of fresh drinking water. In particular, groundwater is susceptible to sea water intrusion; it is known that highly connected 'fast-travel' pathways can exist in the subsurface and often determine the expected time of contamination. By modeling river delta formation and evolution, we tie observations from the surface waterways to the presence of highly connected pathways in the subsurface. Numerical modeling allows us to better understand how these delta systems may respond to different types of sediment inputs and to different steady sea level rise rates. We learn that the surface does indeed provide us some information about the hidden subsurface beneath it, opening up the opportunity for improved modeling of the subsurface from surface information.

## 1 Introduction

River deltas are geologically dynamic and home to large human populations (Syvitski & Saito, 2007; Syvitski et al., 2009; Twilley et al., 2016; Rahman et al., 2019). The changing dynamics of river deltas in response to climate change, upstream river management, and sea level rise threaten both coastal ecosystem health and the lives of millions of people worldwide (Syvitski et al., 2009; Rahman et al., 2019). Thus, it is critical to advance our knowledge and understanding of these geologic systems to help plan and adapt for impending change. One of the resources being threatened is potable groundwater, the primary source of drinking water for 1.5 to 2.8 billion people (Morris et al., 2003). Within aquifers, the connectedness of high permeability facies has long been known to strongly influence flow and solute transport (Fogg, 1986). By understanding the connectedness of the subsurface, groundwater models can be better constrained (Hovadik & Larue, 2010), but the characterization of the subsurface can be challenging due to sparse data limiting our capability of planning for and managing future changes. The subsurface, however, is the result of surface dynamics through time, and, relative to the subsurface, surface spatial data are abundant. Therefore, the characterization of subsurface architecture regimes from surface analysis may provide opportunities to constrain estimates of shallow aquifer connectedness; we explore this idea in this study.

A large body of work has been devoted to the study and analysis of river delta growth and evolution. Studies have focused on the characterization and description of distributary channel networks (Edmonds et al., 2011; Shaw et al., 2013; Ke et al., 2019), the growth and evolution of delta shorelines (Kim et al., 2006; Shaw et al., 2008; Geleynse et al., 2012), and the influence of various external forcings, such as changes to the base level on delta growth and evolution (Koss et al., 1994; Parker et al., 2008; Martin et al., 2009). The control and influence of input sediment properties on delta formation has also been evaluated and quantified (Orton & Reading, 1993; Edmonds & Slingerland, 2010; Burpee et al., 2015). Additionally, global studies have begun to evaluate river deltas across the world to examine their properties and estimate their future morphologies (Giosan et al., 2014; Caldwell et al., 2019; Nienhuis et al., 2020).

Many deltaic systems, such as the Mississippi River Delta and the Ganges-Brahmaputra-Meghna Delta, contain naturally occurring arsenic in shallow subsurface aquifers (Yang et al., 2014; Ayers et al., 2016). These aquifers also face the ever-present threat of saltwater intrusion as both groundwater pumping and sea level rise move the salt-fresh water boundary inland (Moser et al., 2012; Rahman et al., 2019). Predicting groundwater aquifer contamination is further complicated by the fact that many of these coastal aquifers are highly heterogeneous (Winkel et al., 2008; Khan et al., 2016).

To quantify the structure of the subsurface, static (geometrically-based) metrics are used. The basis for this type of metric is connected cluster analysis, a class of methods that can be used to characterize the arrangement of highly permeable facies within the subsurface (Gawlinski & Stanley, 1981; King, 1990). Metrics associated with cluster analysis include the number of clusters, cluster size, and cluster shape and extent relative to the entire field (Renard & Allard, 2013). For example, one measure of bulk connectivity in the subsurface is the ratio of the largest connected cluster volume to the volume of all clusters (Hovadik & Larue, 2007, 2010).

The shape and arrangement of the subsurface are influenced by the surface processes that formed it. In natural river deltas, relating surface processes to subsurface form is complicated by a wide variety of factors as well as the limited time span over which observations are available. Evidence from the stratigraphic record has been used to develop theoretical models for deltaic deposits formed under different base level conditions (G. Allen & Mercier, 1988; Postma, 1995). Many physical and numerical experiments have been designed to test these theoretical models, as well as to measure morphological properties of the surface as the delta deposit is formed (e.g., Koss et al., 1994; Heller et al., 2001; Martin et al., 2009; Geleynse et al., 2012). These studies provide evidence that allogenic forcings influence surface morphology and leave behind identifiable stratigraphic sequences, however the identification of direct relationships between surface morphology and subsurface form remains under-explored.

To interrogate overall patterns and more broad evolutionary trends related to deltaic growth, simplified modeling can be employed (Paola, 2011). The advantage of simplified numerical models over their fully physical counterparts is two-fold: the computational cost of solving simplified physics is lower and simpler models are easier to understand, apply, and analyze. Simplified models have been developed to understand, for example, the lobate growth of delta landforms (Seybold et al., 2007; Moodie et al., 2019). Established models have been modified to explore the influence that multiple variables such as waves and sea level rise (Ratliff et al., 2018), mud and vegetation (Lauzon & Murray, 2018), and ice and permafrost (Lauzon et al., 2019) have on delta morphology and dynamics. In contrast to physical experiments, numerical models allow more experiments to be conducted and therefore additional conditions and forcings to be tested.

In this study, we pursue two main goals. First, we qualitatively explore the influence of input sand fraction (ISF) and sea level rise (SLR) on the surface with a suite of morphologic metrics, and in the subsurface by using geometry-based, static subsurface metrics. Second, we quantitatively identify the metrics most sensitive to ISF and SLR by using the Kullback-Leibler divergence. We employ the numerical model DeltaRCM to simulate surface processes and generate stratigraphy. Inferring knowledge about the subsurface from surface information creates new opportunities to better inform groundwater models and reduce uncertainty around predictions of aquifer and well contamination. In a companion paper, we explore the relationship between these static subsurface metrics and groundwater dynamics (Xu et al., accepted).

## 2 Methods

### 2.1 Description of DeltaRCM

We model delta evolution using DeltaRCM, a hydro-morphodynamic reduced-complexity model that uses empirical rules and weighted random walks to mimic the transport of water and sediment (Liang, Voller, & Paola, 2015; Liang, Geleynse, et al., 2015). DeltaRCM simulates the deposition, erosion, and reworking of two sediment facies: a fine 'mud' sediment that is transported in suspension, and a coarse 'sand' sediment that is transported as bedload. A brief overview of how DeltaRCM routes sediment and develops stratigraphy is presented herein; for a more thorough description we refer the reader to Liang, Voller, and Paola (2015) and Liang, Geleynse, et al. (2015).

The DeltaRCM domain is initialized with an empty basin and a single inlet. Inlet discharge is discretized into parcels of water and sediment which move across the domain via a weighted random walk. The quantity of water and sediment per parcel is a function of the input discharge and the number of parcels specified; here we use 2000 parcels for both water and sediment, in agreement with the number of parcels recommended to balance handling of extreme events and computational cost (Liang, Voller, & Paola, 2015). First the water parcels are routed through the domain to compute a flow field based on the current topography. After the flow field has been computed, the sediment parcels are routed and bed elevations are modified as sediment is eroded and deposited. The partitioning of sediment into individual sand and mud parcels is dictated by the input sediment ratio. In this work, the proportion of input sediment varies between 30% and 70% sand content, with the remainder of the sediment as mud. Physical properties of the sediment follow those of Liang, Voller, and Paola (2015).

The random walk weights are determined by reduced-complexity equations modeled after known physical relationships governing the transport of water and sediment. Fine 'mud' and coarse 'sand' sediment are approximated by varying the properties associated with the transport of these materials such that the fine mud is more easily transported than the coarse sand (see Text S2 and Liang, Voller, and Paola (2015) for further details). The DeltaRCM methodology for simulating river delta dynamics was validated against field data from the Wax Lake Delta and physical experiment data (Liang, Voller, & Paola, 2015; Liang, Van Dyk, & Passalacqua, 2016). The flow routing method was compared to numerical simulations conducted using Delft3D, which solves the discretized Navier-Stokes equations (Liang, Geleynse, et al., 2015).

### 2.2 Model Setup and Numerical Experiments

We conducted a set of 240 numerical experiments to simulate the evolution of river deltas under a variety of scenarios. The inlet conditions, basin geometry, and physical parameters were chosen based on the runs in Liang, Van Dyk, and Passalacqua (2016) (Table 1). All model runs simulated 500 years of delta growth, assuming 10 days of bankfull discharge per year (Caldwell & Edmonds, 2014), absent effects of tides, wind, waves, and subsidence. Three input sand fraction (ISF) scenarios were considered: 30%, 50% and 70% sand by volume in order to capture the variability present in natural systems. For example, bedload fraction estimates for the Ganges and Brahmaputra rivers range from 5 to 50% (Islam et al., 1999), and sand fraction estimates within the Yellow River are around 70% (Li et al., 1998; Edmonds & Slingerland, 2010). For each ISF case, we simulated eight steady sea level rise (SLR) scenarios: 0, 5, 10, 20, 30, 40, 50, and 60 mm/yr, to encompass rates indicative of current and future climatic conditions. Global mean sea level rise rates have been below 10 mm/yr for the past 100 years, however projected mean sea level rise rates are as high as 41 mm/yr by the end of the 21st century (Stocker et al., 2013). The model domain is rectangular and is composed of 50 m x 50 m square grid cells. The vertical depth of each cell in the preserved stratigraphy is 0.05 m. The extents of the domain vary with the SLR rate imposed to best accommodate the final delta extent, while minimizing computational cost. For each scenario (Table 2), we analyzed surface metric trends over six model runs to capture the range of behavior present for a given scenario due to the stochastic variability of DeltaRCM (Liang, Kim, & Passalacqua, 2016; Liang, Van Dyk, & Passalacqua, 2016; Lauzon & Murray, 2018; Lauzon et al., 2019).

| Model Parameter | Value | Units |
|---|---|---|
| Cell Size | 50 x 50 | m |
| Inlet Channel Width | 250 | m |
| Inlet Water Discharge | 1,250 | $m^3/s$ |
| Inlet Channel Depth | 5 | m |
| Inlet Sediment Discharge | 1.25 | $m^3/s$ |
| Basin Depth | 5 | m |
| Threshold dry cell depth | 0.1 | m |
| Time Step Size | 0.0289 | yrs |
| Number of Time Steps | 17,300 | # |
| Initial Sea Level | 0 | m |
| Number of Water Parcels | 2000 | # |
| Number of Sediment Parcels | 2000 | # |
| Topographic Diffusion Coefficient | 0.1 | # |
| Inlet (Reference) Velocity | 1 | m/s |
| Sand Erosion Velocity Threshold | 1.05 | m/s |
| Mud Erosion Velocity Threshold | 1.5 | m/s |
| Mud Deposition Velocity Threshold | 0.3 | m/s |
| Sand Parcel Depth Dependence Exponent ($\theta_{sand}$) | 2 | # |
| Mud Parcel Depth Dependence Exponent ($\theta_{mud}$) | 1 | # |

**Table 1.** DeltaRCM Model Parameter Values

| Run ID | Input Sediment Proportion | Sea Level Rise Rate |
|---|---|---|
| S30R00 | 30% Sand, 70% Mud | 0 mm/yr |
| S30R05 | 30% Sand, 70% Mud | 5 mm/yr |
| S30R10 | 30% Sand, 70% Mud | 10 mm/yr |
| S30R20 | 30% Sand, 70% Mud | 20 mm/yr |
| S30R30 | 30% Sand, 70% Mud | 30 mm/yr |
| S30R40 | 30% Sand, 70% Mud | 40 mm/yr |
| S30R50 | 30% Sand, 70% Mud | 50 mm/yr |
| S30R60 | 30% Sand, 70% Mud | 60 mm/yr |
| S50R00 | 50% Sand, 50% Mud | 0 mm/yr |
| S50R05 | 50% Sand, 50% Mud | 5 mm/yr |
| S50R10 | 50% Sand, 50% Mud | 10 mm/yr |
| S50R20 | 50% Sand, 50% Mud | 20 mm/yr |
| S50R30 | 50% Sand, 50% Mud | 30 mm/yr |
| S50R40 | 50% Sand, 50% Mud | 40 mm/yr |
| S50R50 | 50% Sand, 50% Mud | 50 mm/yr |
| S50R60 | 50% Sand, 50% Mud | 60 mm/yr |
| S70R00 | 70% Sand, 30% Mud | 0 mm/yr |
| S70R05 | 70% Sand, 30% Mud | 5 mm/yr |
| S70R10 | 70% Sand, 30% Mud | 10 mm/yr |
| S70R20 | 70% Sand, 30% Mud | 20 mm/yr |
| S70R30 | 70% Sand, 30% Mud | 30 mm/yr |
| S70R40 | 70% Sand, 30% Mud | 40 mm/yr |
| S70R50 | 70% Sand, 30% Mud | 50 mm/yr |
| S70R60 | 70% Sand, 30% Mud | 60 mm/yr |

**Table 2.** Run IDs, Input Sediment Proportions, and Sea Level Rise Rates

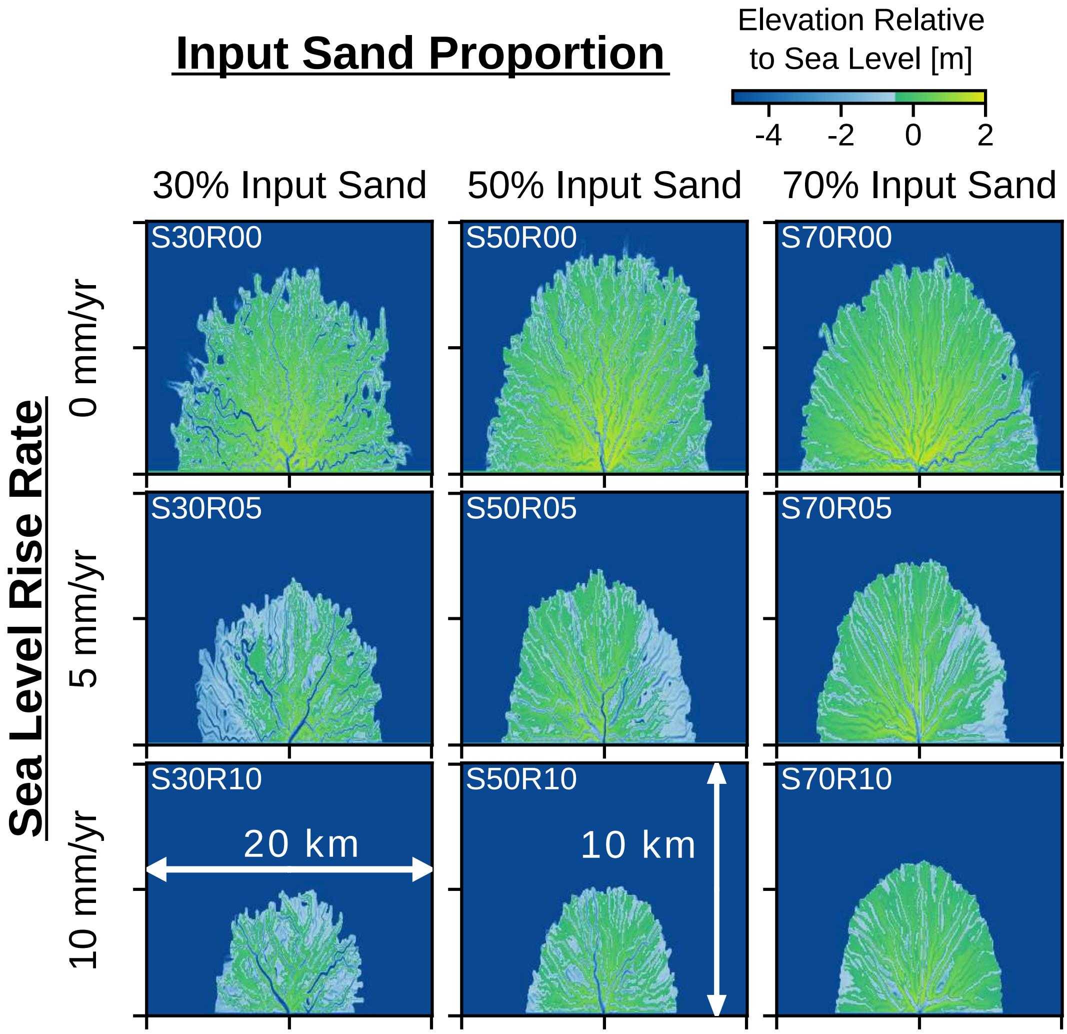


**Figure 1.** DeltaRCM simulated deltas. Representative final topographies of the lower (0, 5, and 10 mm/yr) SLR scenarios.

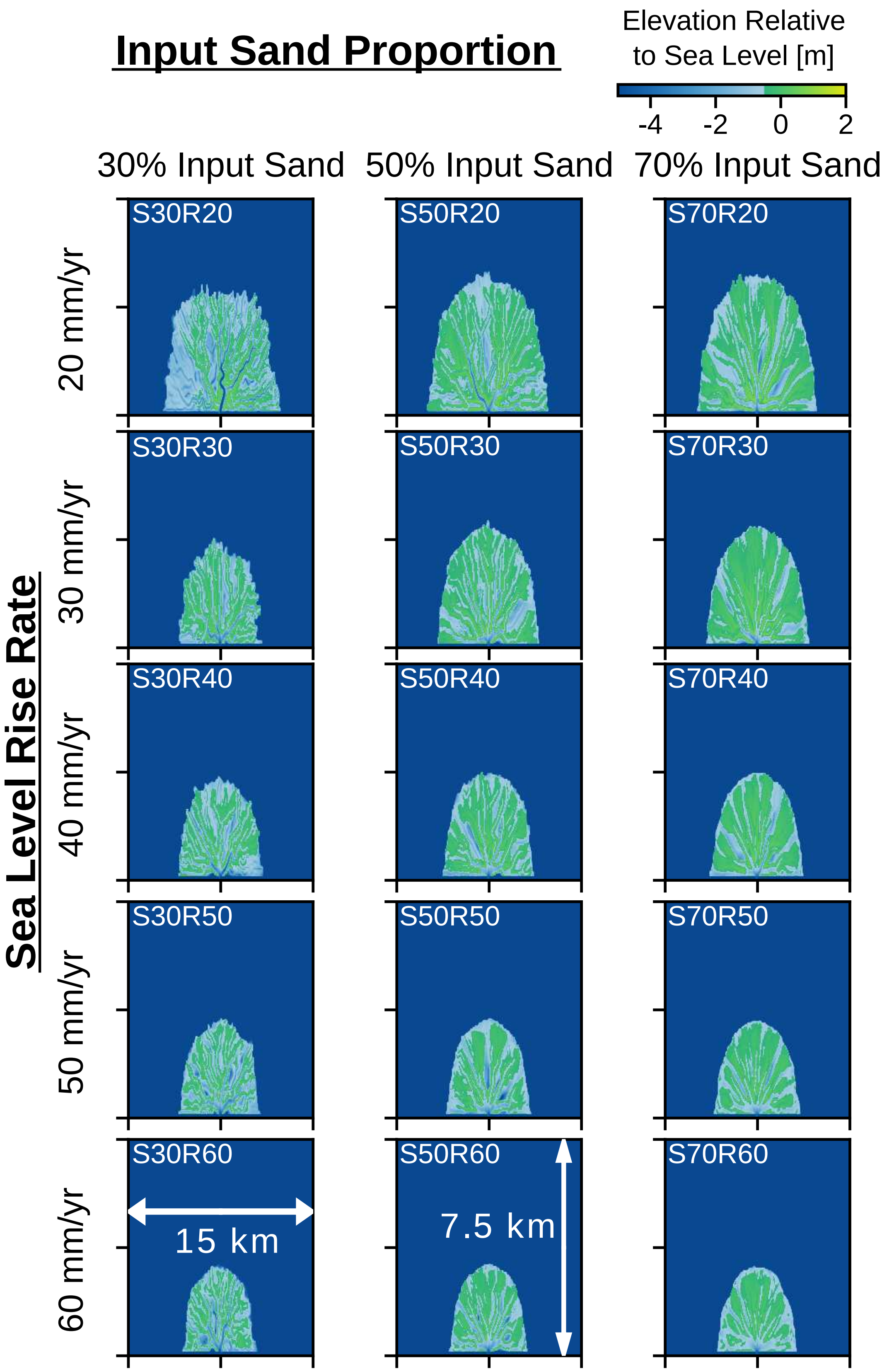


**Figure 2.** DeltaRCM simulated deltas. Representative final topographies of the higher (20, 30, 40, 50, and 60 mm/yr) SLR scenarios.

For the subsurface analysis, model runs with SLR rates greater than 30 mm/yr were extended to a final runtime of 720 years to generate stratigraphic sections with a thickness several times greater than the average sand body thickness (2-3 meters) for the groundwater modeling conducted in the companion study (Xu et al., accepted). Model simulations conducted with SLR rates at and below 30 mm/yr, however, lack the accommodation required to create deep stratigraphic deposits, so we adapted the image quilting (IQ) algorithm (Efros & Freeman, 2001) to join sections of the modeled stratigraphy (Text S1). This technique has been successfully applied to both stationary and non-stationary geological domains (Mahmud et al., 2014; Hoffimann et al., 2017). The forcing scenarios considered are steady in time and produce stratigraphy that is vertically stationary, so rather than using a training image, we employ the 'stitching' portion of the IQ workflow from Mahmud et al. (2014) to vertically join modeled sections of stratigraphy with minimal discontinuities at the boundaries (Figure 3). In this way, the influence of the modeled surface processes on the stratigraphy is kept intact and the bulk properties of the deposit are unchanged (Figure S4), but the depth of the stratigraphic volumes is extended allowing groundwater modeling to be performed.

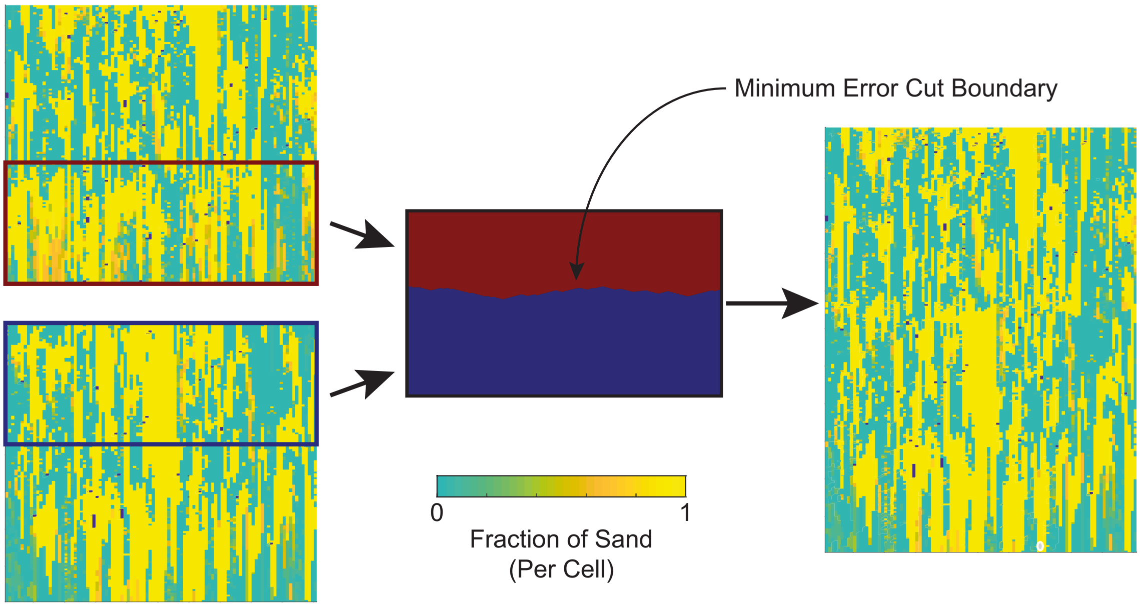


**Figure 3.** Example in 2-D of the 'stitching' procedure adapted from image quilting. First an overlap region is defined within which a minimum error cut boundary is defined (black box). Then the two pieces of stratigraphy are joined along that boundary to form a new image which has a greater depth than either of its constituent sections.

To avoid boundary effects created by the inlet condition and to increase the statistical stationarity of the subsurface domain under study, a rectangular volume is cut from the modeled stratigraphy (Figure 4). We used dimensionless mass extraction parameters (Strong et al., 2005) to determine the lateral extents of this subdomain: in the downstream direction, 30% of the volume from the inlet and 10% of the volume closest to the shoreline are disregarded; perpendicular to the downstream direction, the outer 50% of the volume is excluded (Figure 4). In the vertical direction, the central 25 m from the IQ realizations (0-30 mm/yr SLR scenarios) is used. For the modeled domains from higher SLR scenarios (40-60 mm/yr) the top 5 m of channelized surface and bottom 7.5 m from the initial deposit are excluded (Figure 4).

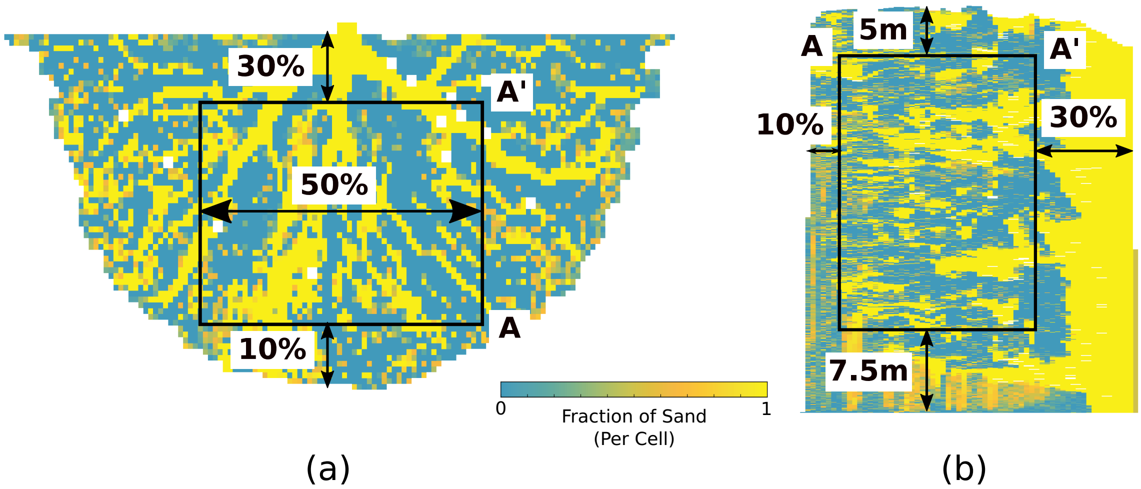


**Figure 4.** Example of the subsurface subdomain over which the subsurface metrics are computed, (a) depicts the lateral extents of the subdomain, and (b) depicts the vertical extents.

### 2.3 Model Output Quantification: Surface Metrics

Several metrics have been proposed and applied to real and simulated river deltas. These metrics were developed to characterize delta morphology and quantify the effect of different processes. We identify 10 of these metrics based on previous work and on their applicability to real systems (Kim & Paola, 2007; Seybold et al., 2007; Wolinsky et al., 2010; Edmonds et al., 2011; Reitz & Jerolmack, 2012; Passalacqua et al., 2013; Van de Lageweg et al., 2013; Liang, Van Dyk, & Passalacqua, 2016; Perignon et al., 2020), and apply them to the numerical modeling results. Metric names, brief descriptions, and sources are provided below and in Table 3. Surface metrics are computed for the years 100-500 of the model runs to avoid measuring properties associated with initial stages of delta formation (Piliouras et al., 2021).

To compute the surface metrics, we obtain a set of binary masks following methods described in Liang, Kim, and Passalacqua (2016) and Lauzon et al. (2019). The shoreline was identified using the opening angle method (Shaw et al., 2008), with a search angle of 75 degrees (after Liang, Kim, & Passalacqua, 2016). This shoreline extraction is based on topographic thresholding using a threshold value 0.5 m below the sea level, to include the shallow subaqueous land after Liang, Kim, and Passalacqua (2016) and Liang, Van Dyk, and Passalacqua (2016). Channel network identification is based on the water velocity fields. The binary channel network is identified as the locations where the water velocity exceeds 0.3 m/s, the minimum velocity required to mobilize sediment, after Liang, Kim, and Passalacqua (2016) and Lauzon et al. (2019). Example shorelines, water velocity fields, and extracted channel networks are provided in Figure S3.

#### *2.3.1 Channel Density*

Channel density (or channelized fraction) is the ratio of channelized area to the total delta topset area (Wolinsky et al., 2010; Liang, Van Dyk, & Passalacqua, 2016). This metric is known to correlate with both input sediment concentration and relative sea level rise rates (Liang, Van Dyk, & Passalacqua, 2016). Under constant forcing conditions, channel density for a mature delta is expected to fluctuate around a constant value (Wolinsky et al., 2010; Reitz & Jerolmack, 2012).

#### *2.3.2 Land Area*

The land area is measured as the total subaerial and shallow subaqueous area (up to 0.5 m below sea level) of the delta topset (Liang, Kim, & Passalacqua, 2016; Liang, Van Dyk, & Passalacqua, 2016). Land area is known to be influenced by both SLR (Muto & Steel, 1997) and ISF (Straub et al., 2015). When there is no base level change and offshore water depth is constant, linear land area growth is expected (Wolinsky et al., 2010).

#### *2.3.3 Channel Depth*

In meandering river systems, the thickness of preserved deposits has been linked to channel morphology, in particular to channel depth (Van de Lageweg et al., 2013). Delta systems contain a variety of channel features, including meanders, making this metric a potential indicator of subsurface structure. Using model outputs, channel depth values are queried at all channel locations and used to compute distributions of water depth in the channels.

#### *2.3.4 Fractal Dimension*

Fractal dimension is an indicator of how self-similar a delta system is and can be used to suggest the presence of a space filling network or a single channel dominated system (Edmonds et al., 2011). This metric is computed, using a box counting approach (Rodriguez-Iturbe et al., 1998), across the different model runs to develop distributions of its values.

#### *2.3.5 Shoreline Roughness*

Shoreline roughness is the ratio of the shoreline length to square root of the delta surface area. This metric is known to reflect sediment input characteristics, waves, and tidal effects (Caldwell & Edmonds, 2014; Liang, Van Dyk, & Passalacqua, 2016). The shoreline roughness metric provides insight into how evenly the system is delivering sediment at the shoreline.

#### *2.3.6 Nearest Edge Distance*

Nearest edge distance is the shortest distance from every land point to a water-land interface or edge (Edmonds et al., 2011). We compute the full distribution of nearest edge distance values as a potential indicator of different geomorphic regimes influencing the spatial arrangement of land and water. In real systems, nearest edge distance has been used to differentiate portions of a delta subject to different processes (Passalacqua et al., 2013).

#### *2.3.7 Island Area and Island Shape Factor*

Delta islands are defined as land masses bounded by channels. We extract islands from model topographies and compute their areas and shape factors (ratio of perimeter to square root of the area). In real delta systems, island properties have been found to be related to channel processes (Edmonds et al., 2011; Piliouras & Rowland, 2020; Perignon et al., 2020). The link between island properties and morphologic activity suggests a potential relationship between surface island morphology and subsurface architecture.

#### *2.3.8 Wetted Fraction and Wet Edge Distance*

The wetted fraction is the ratio of wet area to total delta surface area. Wet pixels, unlike channelized pixels, include former channels that have yet to infill and contain

| Metric Name | Description | Reference |
|---|---|---|
| Channel Density | Proportion of delta surface that is occupied by channels (also called 'channelized fraction') | (Wolinsky et al., 2010; Reitz & Jerolmack, 2012; Liang, Van Dyk, & Passalacqua, 2016) |
| Land Area | Subarial area of delta planform | (Wolinsky et al., 2010; Liang, Van Dyk, & Passalacqua, 2016) |
| Channel Depth | Distribution of water depths in channels | (Van de Lageweg et al., 2013) |
| Fractal Dimension | Fractal dimension of the centerline of the channel network | (Seybold et al., 2007; Edmonds et al., 2011) |
| Shoreline Roughness | Ratio of shoreline length to the square root of delta area | (Wolinsky et al., 2010; Liang, Van Dyk, & Passalacqua, 2016) |
| Nearest Edge Distance | Distribution of distances from a point on land to the nearest water body | (Edmonds et al., 2011; Passalacqua et al., 2013) |
| Island Area | Distribution of areas of deltaic islands | (Edmonds et al., 2011; Perignon et al., 2020) |
| Island Shape Factor | Distribution of the ratio of wetted perimeter of island to the square root of island area | (Passalacqua et al., 2013; Perignon et al., 2020) |
| Wet Edge Distance | Total length of wet-dry interface | (Wolinsky et al., 2010; Liang, Van Dyk, & Passalacqua, 2016) |
| Wetted Fraction | Fractional area covered by all water bodies | (Wolinsky et al., 2010; Reitz & Jerolmack, 2012; Liang, Van Dyk, & Passalacqua, 2016) |

**Table 3.** List of Surface Metrics Measured

water below the channelization threshold velocity (Wolinsky et al., 2010; Liang, Van Dyk, & Passalacqua, 2016). The wetted fraction is thus an indicator of surficial water relative to land mass and can differ significantly from the channelized fraction when many lakes and marshes are present. The wet fraction is expected to vary with a periodicity dictated by delta autogenics (Kim & Paola, 2007; Kim & Jerolmack, 2008). The wet edge distance is the total measure of the edges of channels, lakes, and other water bodies, and has been found to grow even after the wetted fraction becomes constant (Wolinsky et al., 2010).

## 2.4 Model Output Quantification: Subsurface Metrics

Several metrics have been proposed to analyze synthetic stratigraphy and seismic data. Subsurface metrics are typically harder to compute than surface metrics for real systems due to constraints in data acquisition. For this reason, we test 9 different metrics of varying practicality and ease of measurement in the field, ranging from full 3-D sand body identification to 1-D sand package thicknesses (measurable from core data) (Table 4).

### *2.4.1 3-D Geobody Volumes*

The subsurface volume is transformed into a binary structure using a threshold of 80% sand per cell to define 'permeable' and 'impermeable' cells. Once the binary transformation has been completed, we use a connected component analysis to define the volume of each cluster of connected permeable cells. These connected cells (geobodies) are defined as cells which share a face (Pardo-Igúzquiza & Dowd, 2003; Renard & Allard, 2013). We compute the probability distribution of the 3-D geobody volumes for each modeling scenario.

### *2.4.2 2-D Section Geobody Connectivity*

Three orientations of 2-D sections are used to evaluate geobody connectivity: strike, dip, and horizontal. Strike sections are defined as 2-D stratigraphic sections taken perpendicular to the direction of the inlet channel; dip sections are 2-D stratigraphic sections taken parallel to the inlet channel; horizontal sections are plan view slices of the stratigraphic volume. For each section, we identify connected geobodies as those regions with 'permeable' cells that share an edge. The area of the largest geobody divided by the sum of all of the geobody areas in the section defines geobody connectivity (Hovadik & Larue, 2007).

### *2.4.3 2-D Section Percolated Path Ratio*

For the 2-D sections, percolated geobodies are defined as those which connect two opposite boundaries. The sum of the total areas of percolated geobodies divided by the sum of all geobody areas in the section defines the percolated path ratio. For the dip, strike, and horizontal section orientations, we calculated this metric for every 2-D section available in the model subdomains.

### *2.4.4 Sand Package Thickness Distribution and "Connectivity"*

From each modeled subsurface volume, 100 randomly located 1-D 'core' samples are obtained. The thickness of continuous sand packages in each core is recorded and used to develop distributions of sand package thicknesses. In addition, we adapted the first-order measure of connectivity (Hovadik & Larue, 2007) to 1-D by taking the ratio of the largest continuous sand package per core to the total amount of sand.

| Metric Name | Description | Data Dimensionality | Reference |
|---|---|---|---|
| Geobody Volume | Distribution of volumes of connected sand parcels in the stratigraphy | 3-D | (Hovadik & Larue, 2007; Renard & Allard, 2013) |
| Dip Section Connectivity | Ratio of largest geobody area to total summed area of geobodies in a dip section | 2-D | (Hovadik & Larue, 2007) |
| Dip Section Percolated Path Ratio | Ratio of the total area of percolated geobodies to the total area of all geobodies in a dip section | 2-D | (Renard & Allard, 2013) |
| Strike Section Connectivity | Ratio of largest geobody area to total summed area of geobodies in a strike section | 2-D | (Hovadik & Larue, 2007) |
| Strike Section Percolated Path Ratio | Ratio of the total area of percolated geobodies to the total area of all geobodies in a strike section | 2-D | (Renard & Allard, 2013) |
| Horizontal Section Connectivity | Ratio of largest geobody area to total summed area of geobodies in a horizontal section | 2-D | (Hovadik & Larue, 2007) |
| Horizontal Section Percolated Path Ratio | Ratio of the total area of percolated geobodies to the total area of all geobodies in a horizontal section | 2-D | (Renard & Allard, 2013) |
| Sand Package Thickness | Distribution of vertical thicknesses of sand packages identified in 100 random cores of the subsurface | 1-D | (Hovadik & Larue, 2007) |
| Sand Package Connectivity | Ratio of thickest sand layer to sum of all sand in the core | 1-D | (Hovadik & Larue, 2007) |

**Table 4.** List of Subsurface Quantities Measured

### 2.5 Metric Ranking and Significance: Kullback-Leibler Divergence

Given the number of metrics that we propose in the previous section to quantify different aspects of delta morphology and stratigraphic structure, it is not clear which are the most informative for differentiating among delta systems formed under different conditions. To identify the 'best' metrics or those most indicative of the imposed forcings, we use the Kullback-Leibler (KL) divergence, also known as Relative Entropy (Kullback & Leibler, 1951) as in Perignon et al. (2020). The KL divergence of $Q$ from $P$ is defined as:

$$D_{KL}\left(P||Q\right) = \sum_{x \in X} P(x) \log\left(\frac{P(x)}{Q(x)}\right) \tag{1}$$

where both $Q$ and $P$ are discrete probability distributions (PDFs). $P$ is often referred to as the data distribution, and $Q$ as the reference distribution. If $P$ and $Q$ are identical, then the KL divergence between the two is 0. As the probability distributions increasingly differ in shape and position, the KL divergence value increases (Figure S10). KL divergence values greater than 1 indicate significant differences between the distributions $Q$ and $P$, while values less than 1 indicate that $Q$ and $P$ are similar (Perignon et al., 2020). In this way, the KL divergence can be used to quantify the uniqueness of the delta metrics as they correspond to different ISF and SLR scenarios.

To evaluate the delta metrics in this study, a normalized [0,1] discrete PDF is constructed for each metric. To normalize the metrics, each is divided by the maximum value from the group of scenarios being compared. This normalization results in a [0, 1] discrete PDF for each case while preserving absolute differences between the scenarios being compared. The modeled scenarios are compared in two different ways; the influence of the ISF on delta evolution is tested by holding SLR constant, while the influence of SLR is evaluated by holding the ISF constant. To measure the influence of ISF on metric results, $P$ is represented by a single ISF and $Q$ is represented by the combined PDF of the remaining two ISF scenarios. A similar procedure is adopted to compare the low SLR (0, 5, 10 mm/yr) scenarios in which a single scenario is used to construct $P$ while $Q$ is composed of the remaining two scenarios. For the comparison across all eight SLR scenarios, $P$ is defined by the given scenario and $Q$ is always the no SLR (0 mm/yr) case against which the others are compared.

# 3 Results and Discussion

## 3.1 Relating Surface Metric and Subsurface Metric Responses to Forcings

From the normalized metric PDFs (Figures 5 & 6), we identify those metrics most indicative of the forcings imposed on the system. Trends in surface and subsurface metrics in response to different external forcings are analyzed to make predictions about subsurface properties from surface observations.

### *3.1.1 Influence of Input Sand Fraction*

The three surficial metrics that are indicative of the ISF are channel density, shoreline roughness, and wetted fraction. Under low SLR conditions, the shoreline roughness and wetted fraction metrics are the strongest indicators of differences in ISF, while at higher SLR conditions the channel density and wetted fraction metrics are sensitive to different ISF values (Figures S5, S6). Other metric distributions largely retain their shape and position as ISF is changed. For example, the shape and range of the land area distributions remain the same as ISF is varied (Figure 5). In the absence of SLR, total land area in the model is predominantly dependent on the quantity of sediment input into the system because offshore sources and sinks of sediment from waves and tides are not simulated. This model result differs from experimental studies where sediment cohesion is found to be inversely proportional to sediment retention within the delta (Straub et al., 2015). The increase in channel density as ISF is raised is consistent with results from other studies (Caldwell & Edmonds, 2014; Liang, Van Dyk, & Passalacqua, 2016). High sediment cohesion (low ISF) is known to be related to increased values of shoreline roughness (Edmonds & Slingerland, 2010; Straub et al., 2015). Sediment cohesion stabilizes channels, leading to growth of delta lobes while other regions of the delta may be flooded

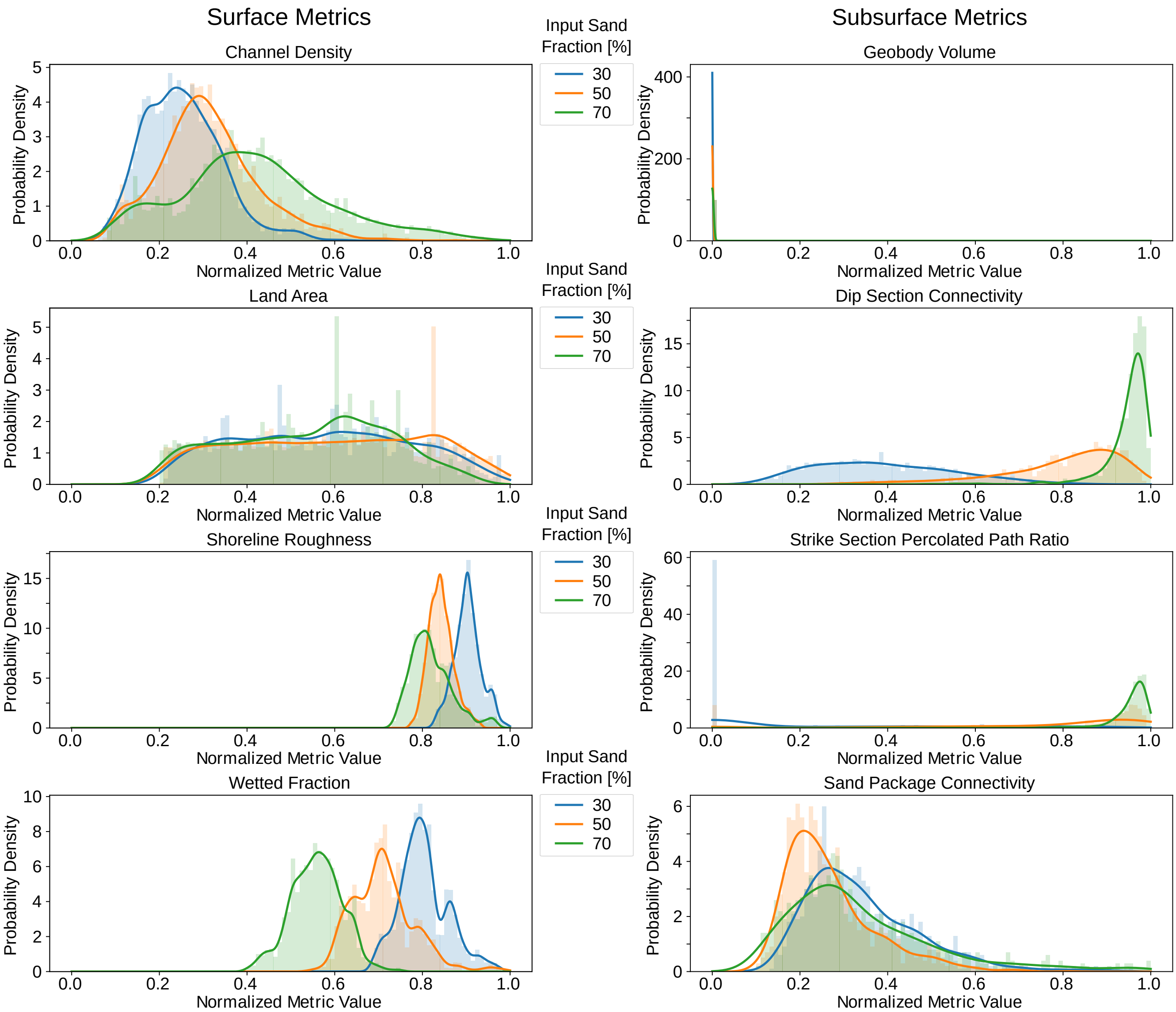


**Figure 5.** Visualization of the influence of ISF on metric values for the 0 mm/yr sea level rise scenarios. Kernel density estimated PDFs are shown overlaid on their source histograms. Normalized histograms for each metric are presented with 100 bins between 0 and 1.

as SLR occurs. This flooding process causes the wetted fraction to decrease as the ISF is increased.

In the subsurface, the most differentiable properties due to variations in input sand content are 2-D section connectivity and percolated path ratio (Figure 5). Normalized distributions of 3-D geobody volume and core sand body thicknesses are largely the same across ISF scenarios due to the presence of many small connected components. These smaller components skew the distributions so severely that they become very similar in shape. Similarly, the percolated path ratio calculated in the strike sections shows evidence of many non-percolated sections for the 30% ISF scenario. Conversely, the 70% ISF scenario has a peak near a percolated path ratio of 1.0, meaning that almost all of the sand is in a geobody that spans the full length of the strike section and connects two opposite boundaries. Dip section geobody connectivity also has visibly different distributions due to differences in ISF (Figure 5). As the ISF into the system increases, we expect geobody connectivity to increase as well. This trend is observed in the dip sections, where the 70% input sand cases have large peaks in connectivity near the value of 1, meaning that the largest geobody in the section includes almost all of the sand. Percolation theory would suggest that between 55 and 60% sand content, the sand bodies in the 2-D sections should be fully connected (King, 1990; Hovadik & Larue, 2007). Although the distribution of sand in deltaic stratigraphy violates many assumptions of percolation theory (random distribution, infinite domain), the connectivity values observed for the 70% ISF scenarios suggest that the mathematical principles from percolation theory can still be applied in geologic settings, a finding consistent with other studies (J. R. Allen, 1978; Donselaar & Overeem, 2008; Pranter & Sommer, 2011).

#### *3.1.2 Influence of Sea Level Rise*

Under different SLR forcing scenarios, delta metrics change in value. On the surface, land area decreases with increasing SLR rate, while channel density increases (Figure 6). The narrowing of the land area PDFs as the rate of SLR increases is indicative of aggradation, while the wide PDF observed for the scenario without any SLR is a signature of progradation. Wetted fraction values increase as the rate of SLR increases, allowing a greater portion of the delta top to be flooded. Shoreline roughness becomes more variable, indicated by wider PDF distributions, in response to increased SLR. Trends in channel density, shoreline roughness, and wetted fraction metrics due to increased SLR are similar to those observed due to changes in ISF (Figure 5).

In the subsurface, several metrics are very similar under all SLR scenarios. 2-D metrics of geobody connectivity in the strike and dip orientations display an initial decrease as SLR increases from 0 to 10 mm/yr (Figure 6). Above the 10 mm/yr SLR rate 2-D connectivity metrics become quite similar, suggesting the existence of a threshold SLR rate above which the preserved deposits maintain a similar level of connectedness. The 1-D analysis of sediment cores shows that sand package connectivity decreases as SLR rate increases (Figure 6). This trend, although subtle, is consistent with the observations of increased shoreline roughness variability and increased channel density on the surface. As surface channels become more numerous and mobile, sand is distributed all over the delta top, resulting in a more even distribution of sand across the platform. The ratio of sand to mud in the system remains the same, however, and the increased spread of sand creates thinner individual sand layers that become segmented by mud.

#### *3.1.3 Applying the Kullback-Leibler Divergence to Metric Differentiation*

The strike and dip section connectivity and percolated path ratio metrics are the most divergent in the subsurface due to changes in ISF (Figure 7a,b). This finding is consistent with the previous observations made from the metric PDFs. On the surface, shore-

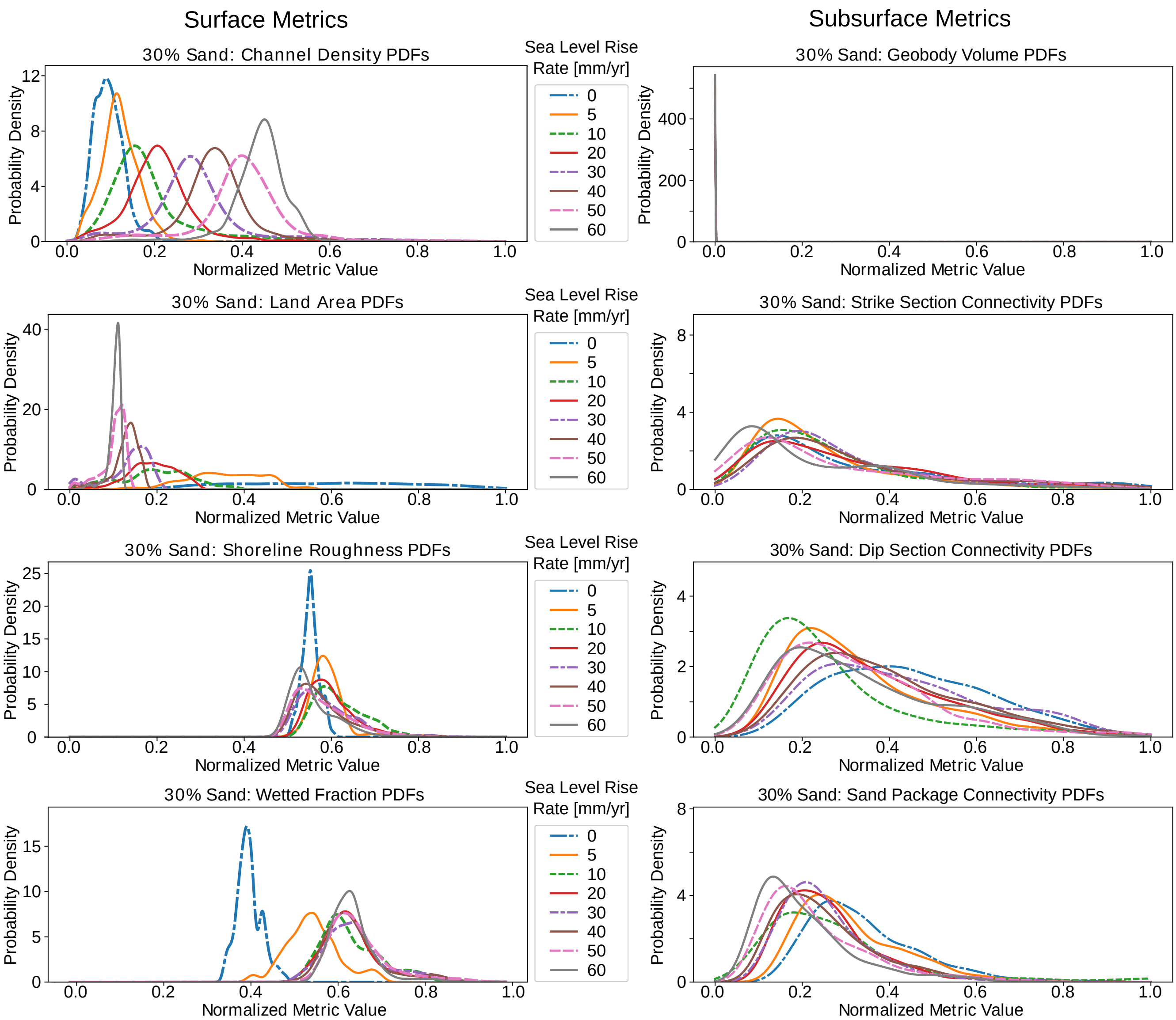


**Figure 6.** Visualization of the influence of SLR on metric values for the 30% ISF scenarios. Kernel density estimated PDFs of normalized metric values are shown for each SLR scenario. Some metrics exhibit clear responses to the different SLR conditions. For example, channel density PDFs (upper left) display a visible response to the SLR forcing, whereas geobody volume PDFs (upper right) are indistinguishable across the different SLR scenarios.

line roughness and wetted fraction are consistently divergent as ISF is varied, even under different SLR conditions. At higher SLR rates channel density, land area, nearest edge distance, and wet edge distance have increasingly large KL divergence values, indicating that these PDFs become more sensitive to ISF when SLR rates are high (Figure 7b).

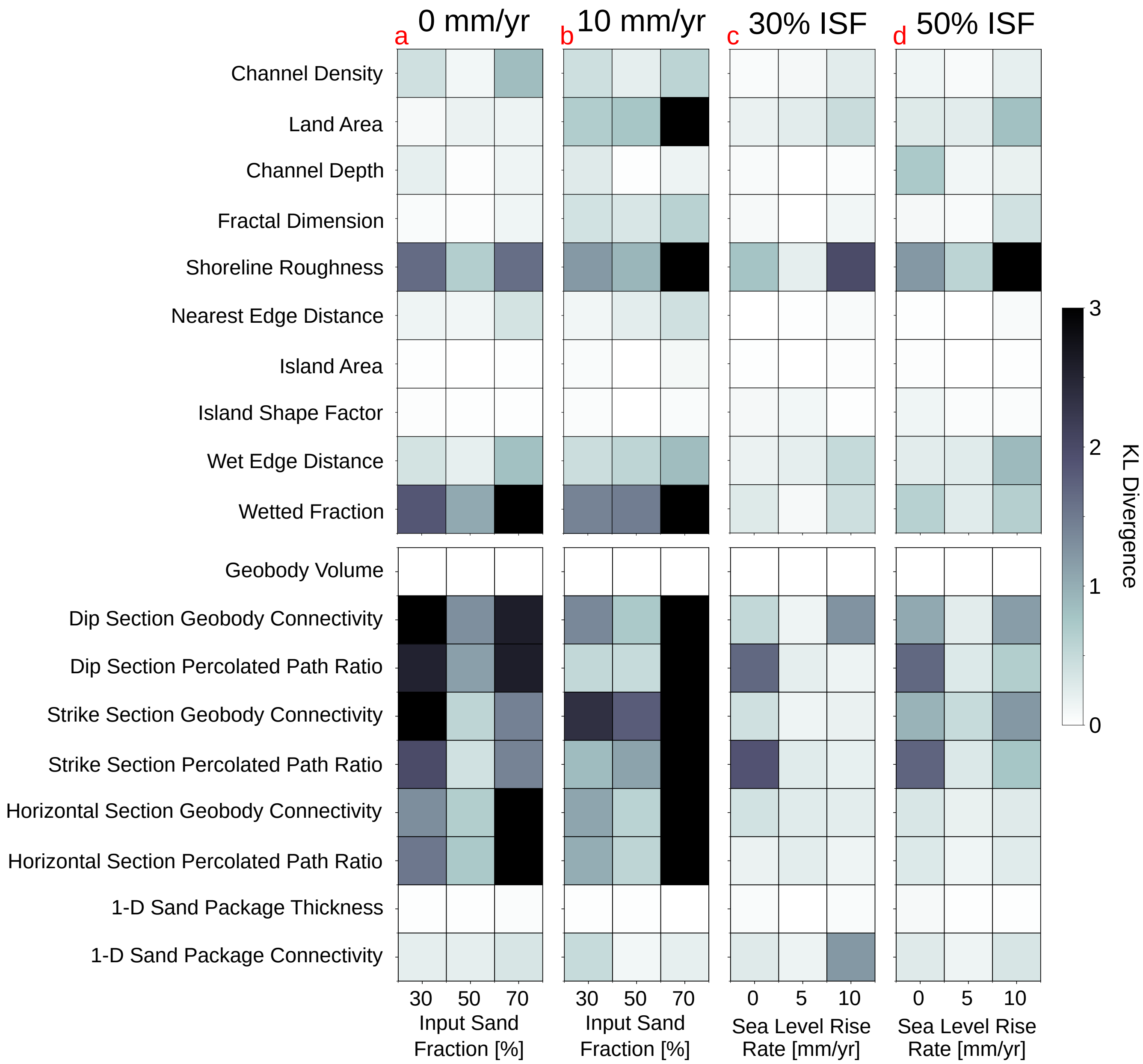


**Figure 7.** Graphic depiction of the KL divergence results. The darkness of the cells indicates the KL divergence value between that metric represented by that cell for that particular scenario and the others in the row. **a**: Differences in metric response due to changes in ISF under no SLR (rise rate of 0 mm/yr). **b**: Differences in metric response due to changes in ISF when sea level rises at a rate of 10 mm/yr. **c**: Metric differences due to SLR for the lowest three sea level rise scenarios examined when ISF is held constant at 30%. **d**: Metric differences due to SLR for the lowest three SLR scenarios examined when ISF is held constant at 50%.

When examining the influence of SLR on metric distributions, we analyzed the 'low' SLR scenarios (0, 5, 10 mm/yr) separately (Figure 7c,d) as well as together with the full range of SLR rates simulated (Figure 8). To better understand the differences among these metrics at lower rates of SLR, we evaluated the 0, 5, and 10 mm/yr cases separately in the same manner as the ISF cases. On the surface, shoreline roughness is a weak metric for distinguishing between these different rates of SLR. In the subsurface, the most distinct metrics are the connectivity and percolated path ratios in the strike and dip sections. Overall, distinctions between subsurface metrics due to SLR are more muted than those due to ISF.

When looking at the full panel of SLR scenarios, metrics like channel density, shoreline roughness, wetted edge distance, and wetted fraction have high divergence values, which is in line with observations made from the PDFs. The change in the land area PDFs as a result of SLR is evident in the KL divergence results, as systems that are smaller and more aggradational show higher KL divergence values than those closer to the reference case (0 mm/yr SLR). As SLR values become increasingly extreme, fractal dimension PDFs at high SLR begin to diverge significantly from the reference (0 mm/yr) SLR case (Figure 8). In the subsurface, 1-D sand package connectivity, strike and dip section connectivity, and percolated path ratios metrics are the most divergent. The distinction between the reference no SLR case, and the 5 and 10 mm/yr SLR cases is made clear by the darker squares, while the lighter squares around 20 and 30 mm/yr suggest that these distributions begin to resemble the reference case again (Figure 8). This behavior is consistent with the initial trend of decreasing connectivity from 0 to 10 mm/yr SLR, and the absence of a trend as SLR rate increased. The differences between distributions of geobody volumes and sand package thicknesses are small, as previously noted, due to the sheer number of small geobody volumes and thin sand packages skewing the distributions. By computing the KL divergence in addition to the metric PDFs shown previously (Figure 6), our qualitative observations are supported by quantitative differences between the different modeled scenarios.

In this study we began to constrain subsurface geometry using surface network information. We focused on river dominated deltas, where the riverine input is the primary driver of the surface and subsurface structure. On the surface, the shoreline roughness and wetted fraction are useful metrics for differentiating between deltas formed under different ISF and SLR conditions. In the subsurface, metrics of connectivity and percolated path ratios computed in the 2-D strike and dip sections are the strongest indicators of different ISF and SLR forcings. With this knowledge we can improve surface metric selection needed to make inferences about stratigraphic properties. The next step towards improving aquifer contamination forecasts is to link properties of subsurface geometry to groundwater flow behavior; this relationship is explored in a companion paper, Xu et al. (accepted).

### 3.2 Study Applicability and Limitations

Using simplified model dynamics allowed us to isolate the effects of ISF and SLR on deltaic evolution. These two forcings are known to have strong controls on river delta morphology (Caldwell & Edmonds, 2014). We find that for river-dominated systems, the surface metrics most sensitive to ISF and SLR are the wetted fraction and shoreline roughness metrics, both of which can be readily calculated from satellite imagery. Wetted fraction values can be calculated from remotely sensed imagery using automated methods for surface water detection (e.g. Isikdogan et al., 2020; Feng et al., 2019), while the opening angle method, used for shoreline detection in this work, was originally applied to satellite imagery (Shaw et al., 2008). These two surface metrics are potential indicators of subsurface connectivity, a metric much more difficult to estimate in real systems. Therefore, these findings may be used in studies that seek to compare the subsurface structure of existing river-dominated systems as they utilize surface information, complementing methods for subsurface estimation based on direct measurements and field data. The KL divergence approach as applied to deltaic metrics is also useful when comparing morphological metrics between different delta experiments.

The deposits modeled in this study are on the order of 10 m thick, and generated over timescales $< 10^3$ years (Figure S2). Although much of this modeled stratigraphy may be reworked, and the corresponding surface signal 'shredded,' over longer geologic timescales (Jerolmack & Paola, 2010; Toby et al., 2019), the structure of the shallow subsurface remains important for those dependent on the groundwater it contains. In the Bengal basin for example, many domestic wells and some irrigation wells are shallower than 50 m, making the near-surface stratigraphy critical for contaminant transport (Michael & Voss, 2009; Bahar & Reza, 2010; Shamsudduha et al., 2011). Groundwater resources may therefore be affected by subsurface features which are not persistent over the geologic record, making studies focused on shorter timescales, such as this one, important when trying to predict the structure of the shallow subsurface as forcings change and landscapes evolve.

Specific forcings not incorporated in the DeltaRCM model include winds, waves, and tides, which are known to have strong effects on delta morphology (Galloway, 1975; Anthony, 2015) and are the dominant forcings in many deltas world-wide (Nienhuis et al., 2020). River-dominated deltas, as analyzed here, tend to be large in size, convey significant quantities of water and sediment, and are home to millions of people (Nienhuis et al., 2020; Edmonds et al., 2020). This study also simplifies the variety of flow conditions present in river deltas by exclusively simulating bankfull discharge conditions, thereby missing processes and reworking which occur during periods of lower flow (Shaw & Mohrig, 2014; Miller et al., 2019). We acknowledge that by not modeling these effects, this study does not capture the full range of deltaic morphology and dynamics. But we believe that our present findings are still useful as complementary methods to other subsurface estimation methods, and serve as a starting point for future studies seeking to link surface and subsurface form in river-dominated deltaic systems experiencing different ISF or SLR conditions.

The division of sediment types into two discrete categories, a fine mud and a coarse sand, simplifies the sediment grain size continuum. The input sediment grain size distribution is known to impact the morphology and subsurface structure of river deltas (Orton & Reading, 1993; Caldwell & Edmonds, 2014). Given the resolution at which the stratigraphy has been modeled (5 cm), this two-facies methodology accelerates model run time, and maintains the reduced-complexity modeling approach. As a result, the results do not reproduce small stratigraphic structures that exist below the modeled resolution such as thin mud drapes, which are often found in deltaic deposits (Galloway, 1976; Tye & Coleman, 1989; Tanabe et al., 2003). In addition, the modeling conducted in this study did not account for the effects of vegetation, permafrost, or ice on deltaic evolution. We note that the DeltaRCM model has been modified to simulate these effects (Lauzon & Murray, 2018; Lauzon et al., 2019; Piliouras et al., 2021), however these modifications were kept out of this study for the sake of simplicity.

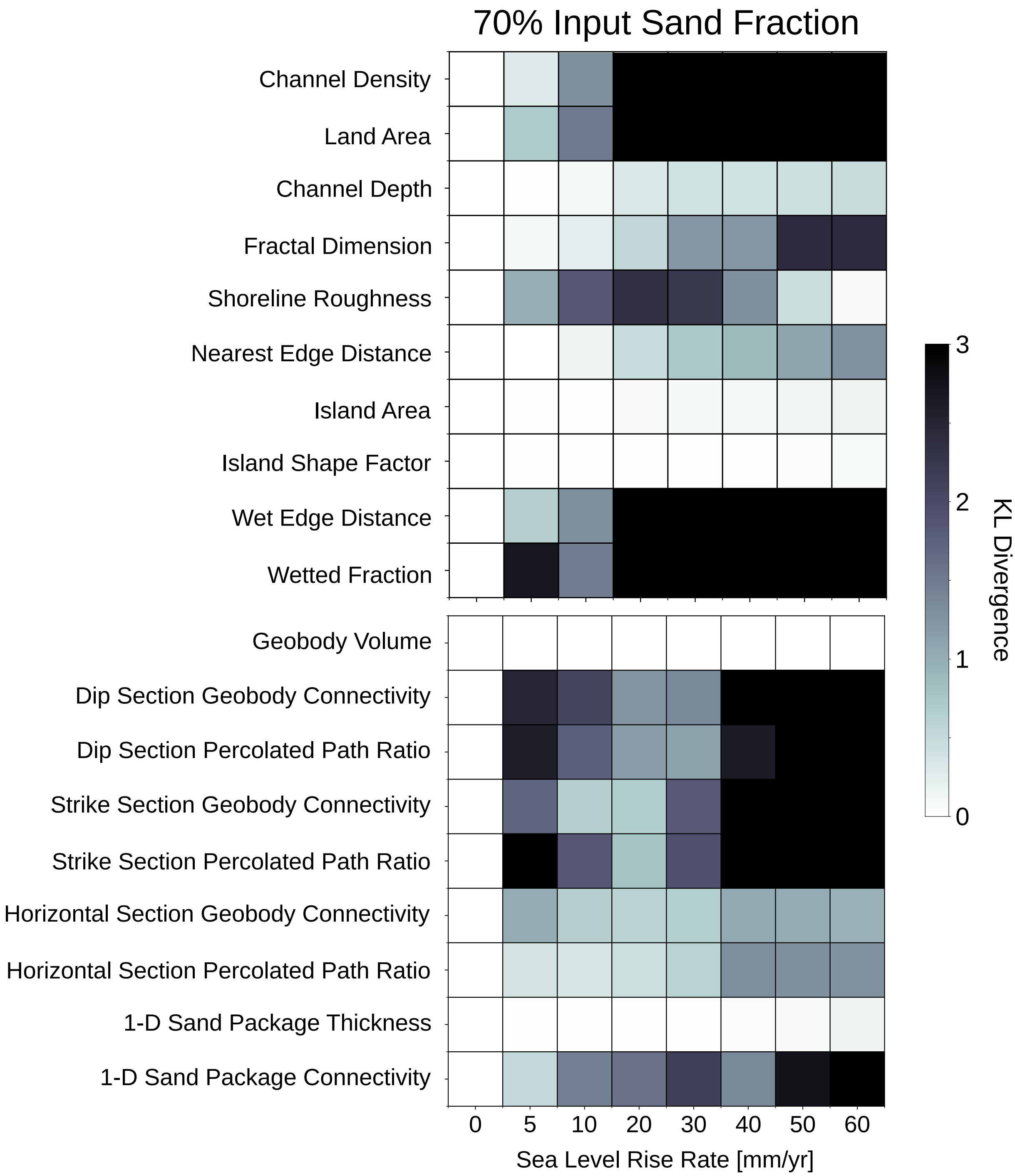


**Figure 8.** Graphic depiction of the KL divergence results computed in reference to the no SLR (0 mm/yr) scenario. Darker cells indicate a greater divergence from the reference, no SLR, scenario. Results shown are for the 70% ISF scenarios.

## 4 Conclusions

In our simulated scenarios we find that information from the surface network can be used to constrain predictions of subsurface structure, however further work needs to be conducted to constrain the applicability of these results to real systems. Broadly, more variable shoreline roughness values and greater wetted fraction values correspond with higher subsurface connectivity. By modeling and evaluating 24 different scenarios of delta growth and evolution, we find that:

1. As ISF increases, wetted fraction, shoreline roughness variability, and subsurface connectivity increase
2. Surface metrics are useful in informing subsurface properties at SLR rates below 10 mm/yr; above this rate the subsurface properties become insensitive to SLR rate
3. Shoreline roughness and wetted fraction consistently prove to be the most effective for differentiating between forcing scenarios of the 10 surface metrics studied
4. Connectivity and percolated path ratio in the strike and dip sections were the most sensitive to changes in forcings of the 9 subsurface metrics evaluated

These findings are supported by both qualitative observations of the metric PDFs, as well as a KL divergence analysis in which the PDFs of the metrics were compared mathematically. This study has shown the potential for surface information to provide insights into subsurface properties, and that mathematical methods such as the KL divergence can be applied to support the choice of metrics to measure.

## Acknowledgments

The authors acknowledge support from the National Science Foundation via EAR-1719670. The DeltaRCM model can be downloaded from the CSDMS model repository at `https://csdms.colorado.edu/wiki/Model:DeltaRCM`.

## References


Allen, G., & Mercier, F. (1988). Subsurface sedimentology of deltaic systems. *PESA J.*, *(12)*, 30–44.

Allen, J. R. (1978, aug). Studies in fluviatile sedimentation: an exploratory quantitative model for the architecture of avulsion-controlled alluvial suites. *Sedimentary Geology*, *21*(2), 129–147. doi: 10.1016/0037-0738(78)90002-7

Anthony, E. J. (2015, mar). *Wave influence in the construction, shaping and destruction of river deltas: A review* (Vol. 361). Elsevier. Retrieved from `https://www.sciencedirect.com/science/article/pii/S0025322714003788` doi: 10.1016/j.margeo.2014.12.004

Ayers, J. C., Goodbred, S., George, G., Fry, D., Benneyworth, L., Hornberger, G., … Akter, F. (2016, dec). Sources of salinity and arsenic in groundwater in southwest Bangladesh. *Geochemical Transactions*, *17*(1), 4. Retrieved from `http://geochemicaltransactions.springeropen.com/articles/10.1186/s12932-016-0036-6` doi: 10.1186/s12932-016-0036-6

Bahar, M. M., & Reza, M. S. (2010, feb). Hydrochemical characteristics and quality assessment of shallow groundwater in a coastal area of southwest Bangladesh. *Environmental Earth Sciences*, *61*(5), 1065–1073. Retrieved from `https://link.springer.com/article/10.1007/s12665-009-0427-4` doi: 10.1007/s12665-009-0427-4

Burpee, A. P., Slingerland, R. L., Edmonds, D. A., Parsons, D., Best, J., Cederberg, J., … Royce, J. (2015, jun). Grain-size controls on the morphology and internal geometry of river-dominated deltas. *Journal of Sedimentary Research*, *85*(6), 699–714. Retrieved from `http://dx.doi.org/10.2110/jsr.2015.39` doi: 10.2110/jsr.2015.39

Caldwell, R. L., & Edmonds, D. A. (2014, may). The effects of sediment properties on deltaic processes and morphologies: A numerical modeling study. *Journal of Geophysical Research: Earth Surface*, *119*(5), 961–982. Retrieved from `http://doi.wiley.com/10.1002/2013JF002965` doi: 10.1002/2013JF002965

Caldwell, R. L., Edmonds, D. A., Baumgardner, S., Paola, C., Roy, S., & Nienhuis, J. H. (2019, aug). A global delta dataset and the environmental variables that predict delta formation on marine coastlines. *Earth Surface Dynamics*, *7*(3), 773–787. Retrieved from `https://www.earth-surf-dynam.net/7/773/2019/` doi: 10.5194/esurf-7-773-2019

Donselaar, M. E., & Overeem, I. (2008, sep). Connectivity of fluvial point-bar deposit: An example from the Miocene Huesca fluvial fan, Ebro Basin, Spain. *American Association of Petroleum Geologists Bulletin*, *92*(9), 1109–1129. Retrieved from `http://pubs.geoscienceworld.org/aapgbull/article-pdf/92/9/1109/3369570/bltn07079.pdf` doi: 10.1306/04180807079

Edmonds, D. A., Caldwell, R. L., Brondizio, E. S., & Siani, S. M. (2020, sep). Coastal flooding will disproportionately impact people on river deltas. *Nature Communications*, *11*(1), 1–8. Retrieved from `https://www.nature.com/articles/s41467-020-18531-4` doi: 10.1038/s41467-020-18531-4

Edmonds, D. A., Paola, C., Hoyal, D. C., & Sheets, B. A. (2011, nov). Quantitative metrics that describe river deltas and their channel networks. *Journal of Geophysical Research: Earth Surface*, *116*(4), F04022. Retrieved from `http://doi.wiley.com/10.1029/2010JF001955` doi: 10.1029/2010JF001955

Edmonds, D. A., & Slingerland, R. L. (2010). Significant effect of sediment cohesion on deltamorphology. *Nature Geoscience*, *3*(2), 105–109. Retrieved from `https://search-proquest-com.ezproxy.lib.utexas.edu/docview/1030084431?pq-origsite=summon` doi: 10.1038/ngeo730

Efros, A. A., & Freeman, W. T. (2001). Image quilting for texture synthesis and transfer. In *Proceedings of the 28th annual conference on computer graphics and interactive techniques, siggraph 2001* (pp. 341–346). New York, New York, USA: ACM Press. Retrieved from http://portal.acm.org/citation.cfm?doid=383259.383296 doi: 10.1145/383259.383296

Feng, W., Sui, H., Huang, W., Xu, C., & An, K. (2019, apr). Water Body Extraction From Very High-Resolution Remote Sensing Imagery Using Deep U-Net and a Superpixel-Based Conditional Random Field Model. *IEEE Geoscience and Remote Sensing Letters*, *16*(4), 618–622. Retrieved from https://ieeexplore.ieee.org/document/8573826/ doi: 10.1109/LGRS.2018.2879492

Fogg, G. E. (1986, may). Groundwater Flow and Sand Body Interconnectedness in a Thick, Multiple-Aquifer System. *Water Resources Research*, *22*(5), 679–694. Retrieved from http://doi.wiley.com/10.1029/WR022i005p00679 doi: 10.1029/WR022i005p00679

Galloway, W. E. (1975). Process framework for describing the morphologic and stratigraphic evolution of deltaic systems. In *Deltas, models for exploration* (pp. 87–98). Houston Geological Society. Retrieved from https://archives.datapages.com/data/hgssp/data/022/022001/87_hgs0220087.htm

Galloway, W. E. (1976, sep). Sediments and Stratigraphic Framework of the Copper River Fan-delta, Alaska. *SEPM Journal of Sedimentary Research*, *Vol. 46*(3), 726–737. Retrieved from http://pubs.geoscienceworld.org/sepm/jsedres/article-pdf/46/3/726/2807555/726.pdf doi: 10.1306/212f703b-2b24-11d7-8648000102c1865d

Gawlinski, E. T., & Stanley, H. E. (1981, aug). Continuum percolation in two dimensions: Monte Carlo tests of scaling and universality for non-interacting discs. *Journal of Physics A: Mathematical and General*, *14*(8), 291–299. Retrieved from https://iopscience-iop-org.ezproxy.lib.utexas.edu/article/10.1088/0305-4470/14/8/007https://iopscience-iop-org.ezproxy.lib.utexas.edu/article/10.1088/0305-4470/14/8/007/meta doi: 10.1088/0305-4470/14/8/007

Geleynse, N., Voller, V. R., Paola, C., & Ganti, V. (2012, sep). Characterization of river delta shorelines. *Geophysical Research Letters*, *39*(17), n/a–n/a. Retrieved from http://doi.wiley.com/10.1029/2012GL052845 doi: 10.1029/2012GL052845

Giosan, L., Syvitski, J., Constantinescu, S., & Day, J. (2014, dec). *Climate change: Protect the world's deltas* (Vol. 516) (No. 729). Nature Publishing Group. doi: 10.1038/516031a

Heller, P. L., Paola, C., Hwang, I. G., John, B., & Steel, R. (2001, may). Geomorphology and sequence stratigraphy due to slow and rapid base-level changes in an experimental subsiding basin (XES96-1). *AAPG Bulletin*, *85*(5), 817–838. Retrieved from http://pubs.geoscienceworld.org/aapgbull/article-pdf/85/5/817/3358382/817.pdf doi: 10.1306/8626ca0f-173b-11d7-8645000102c1865d

Hoffimann, J., Scheidt, C., Barfod, A., & Caers, J. (2017, sep). Stochastic simulation by image quilting of process-based geological models. *Computers and Geosciences*, *106*, 18–32. Retrieved from https://www.sciencedirect.com/science/article/pii/S0098300417301139 doi: 10.1016/j.cageo.2017.05.012

Hovadik, J. M., & Larue, D. K. (2007, aug). *Static characterizations of reservoirs: Refining the concepts of connectivity and continuity* (Vol. 13) (No. 3). Geological Society of London. Retrieved from http://pg.lyellcollection.org/cgi/doi/10.1144/1354-079305-697 doi: 10.1144/1354-079305-697

Hovadik, J. M., & Larue, D. K. (2010). Stratigraphic and structural connectivity. *Geological Society, London, Special Publications*, *347*(1), 219–242. Retrieved from https://sp.lyellcollection.org/content/347/1/219 doi: 10.1144/SP347.13

Isikdogan, L. F., Bovik, A., & Passalacqua, P. (2020, oct). Seeing Through the

Clouds With DeepWaterMap. *IEEE Geoscience and Remote Sensing Letters*, *17*(10), 1662–1666. Retrieved from https://ieeexplore.ieee.org/document/8913594/ doi: 10.1109/LGRS.2019.2953261

Islam, M. R., Begum, S. F., Yamaguchi, Y., & Ogawa, K. (1999, dec). The Ganges and Brahmaputra rivers in Bangladesh: Basin denudation and sedimentation. *Hydrological Processes*, *13*(17), 2907–2923. Retrieved from https://onlinelibrary.wiley.com/doi/10.1002/(SICI)1099-1085(19991215)13:17%3C2907::AID-HYP906%3E3.0.CO;2-E doi: 10.1002/(SICI)1099-1085(19991215)13:17⟨2907::AID-HYP906⟩3.0.CO;2-E

Jerolmack, D. J., & Paola, C. (2010, oct). Shredding of environmental signals by sediment transport. *Geophysical Research Letters*, *37*(19). Retrieved from http://doi.wiley.com/10.1029/2010GL044638 doi: 10.1029/2010GL044638

Ke, W. T., Shaw, J. B., Mahon, R. C., & Cathcart, C. A. (2019, jul). Distributary Channel Networks as Moving Boundaries: Causes and Morphodynamic Effects. *Journal of Geophysical Research: Earth Surface*, *124*(7), 1878–1898. Retrieved from https://onlinelibrary.wiley.com/doi/abs/10.1029/2019JF005084 doi: 10.1029/2019JF005084

Khan, M. R., Koneshloo, M., Knappett, P. S., Ahmed, K. M., Bostick, B. C., Mailloux, B. J., ... Michael, H. A. (2016). Megacity pumping and preferential flow threaten groundwater quality. *Nature Communications*, *7*. Retrieved from https://search-proquest-com.ezproxy.lib.utexas.edu/docview/1823511985?pq-origsite=summon doi: 10.1038/ncomms12833

Kim, W., & Jerolmack, D. J. (2008, jul). The pulse of calm fan deltas. *Journal of Geology*, *116*(4), 315–330. Retrieved from https://www.journals.uchicago.edu/doi/10.1086/588830 doi: 10.1086/588830

Kim, W., & Paola, C. (2007, apr). Long-period cyclic sedimentation with constant tectonic forcing in an experimental relay ramp. *Geology*, *35*(4), 331–334. Retrieved from http://pubs.geoscienceworld.org/gsa/geology/article-pdf/35/4/331/3533089/i0091-7613-35-4-331.pdf doi: 10.1130/G23194A.1

Kim, W., Paola, C., Swenson, J. B., & Voller, V. R. (2006, dec). Shoreline response to autogenic processes of sediment storage and release in the fluvial system. *Journal of Geophysical Research: Earth Surface*, *111*(4), F04013. Retrieved from http://doi.wiley.com/10.1029/2006JF000470 doi: 10.1029/2006JF000470

King, P. R. (1990). The connectivity and conductivity of overlapping sand bodies. *North sea oil and gas reservoirs - II*, 353–362. Retrieved from https://link-springer-com.ezproxy.lib.utexas.edu/chapter/10.1007/978-94-009-0791-1_30 doi: 10.1007/978-94-009-0791-1_30

Koss, J. E., Ethridge, F. G., & Schumm, S. A. (1994, may). An experimental study of the effects of base-level change on fluvial, coastal plain and shelf systems. *Journal of Sedimentary Research B: Stratigraphy & Global Studies*, *64*(B64(2)), 90–98. Retrieved from http://pubs.geoscienceworld.org/sepm/jsedres/article-pdf/64/2b/90/2811439/90.pdf doi: 10.1306/d4267f64-2b26-11d7-8648000102c1865d

Kullback, S., & Leibler, R. A. (1951, mar). On Information and Sufficiency. *The Annals of Mathematical Statistics*, *22*(1), 79–86. doi: 10.1214/aoms/1177729694

Lauzon, R., & Murray, A. B. (2018, oct). Comparing the Cohesive Effects of Mud and Vegetation on Delta Evolution. *Geophysical Research Letters*, *45*(19), 10,437–10,445. Retrieved from https://onlinelibrary.wiley.com/doi/abs/10.1029/2018GL079405 doi: 10.1029/2018GL079405

Lauzon, R., Piliouras, A., & Rowland, J. C. (2019, jun). Ice and Permafrost Effects on Delta Morphology and Channel Dynamics. *Geophysical Research Letters*, *46*(12), 6574–6582. Retrieved from https://onlinelibrary.wiley.com/

doi/abs/10.1029/2019GL082792 doi: 10.1029/2019GL082792

Li, G., Wei, H., Han, Y., & Chen, Y. (1998, aug). Sedimentation in the Yellow River delta, Part I: Flow and suspended sediment structure in the upper distributary and the estuary. *Marine Geology*, *149*(1-4), 93–111. doi: 10.1016/S0025-3227(98)00031-0

Liang, M., Geleynse, N., Edmonds, D. A., & Passalacqua, P. (2015). A reduced-complexity model for river delta formation - Part 2: Assessment of the flow routing scheme. *Earth Surface Dynamics*, *3*(1), 87–104. Retrieved from www.earth-surf-dynam.net/3/87/2015/ doi: 10.5194/esurf-3-87-2015

Liang, M., Kim, W., & Passalacqua, P. (2016, oct). How much subsidence is enough to change the morphology of river deltas? *Geophysical Research Letters*, *43*(19), 10,266–10,276. Retrieved from http://doi.wiley.com/10.1002/2016GL070519 doi: 10.1002/2016GL070519

Liang, M., Van Dyk, C., & Passalacqua, P. (2016, feb). Quantifying the patterns and dynamics of river deltas under conditions of steady forcing and relative sea level rise. *Journal of Geophysical Research: Earth Surface*, *121*(2), 465–496. Retrieved from http://doi.wiley.com/10.1002/2015JF003653 doi: 10.1002/2015JF003653

Liang, M., Voller, V. R., & Paola, C. (2015). A reduced-complexity model for river delta formation - Part 1: Modeling deltas with channel dynamics. *Earth Surface Dynamics*, *3*(1), 67–86. Retrieved from www.earth-surf-dynam.net/3/67/2015/ doi: 10.5194/esurf-3-67-2015

Mahmud, K., Mariethoz, G., Caers, J., Tahmasebi, P., & Baker, A. (2014, apr). Simulation of Earth textures by conditional image quilting. *Water Resources Research*, *50*(4), 3088–3107. Retrieved from http://doi.wiley.com/10.1002/2013WR015069 doi: 10.1002/2013WR015069

Martin, J., Sheets, B., Paola, C., & Hoyal, D. (2009, aug). Influence of steady base-level rise on channel mobility, shoreline migration, and scaling properties of a cohesive experimental delta. *Journal of Geophysical Research: Solid Earth*, *114*(3), F03017. Retrieved from http://doi.wiley.com/10.1029/2008JF001142 doi: 10.1029/2008JF001142

Michael, H. A., & Voss, C. I. (2009, feb). Controls on groundwater flow in the Bengal Basin of India and Bangladesh: Regional modeling analysis. *Hydrogeology Journal*, *17*(7), 1561–1577. Retrieved from https://link.springer.com/article/10.1007/s10040-008-0429-4 doi: 10.1007/s10040-008-0429-4

Miller, K. L., Kim, W., & McElroy, B. (2019, feb). Laboratory Investigation on Effects of Flood Intermittency on Fan Delta Dynamics. *Journal of Geophysical Research: Earth Surface*, *124*(2), 383–399. Retrieved from https://onlinelibrary.wiley.com/doi/abs/10.1029/2017JF004576 doi: 10.1029/2017JF004576

Moodie, A. J., Nittrouer, J. A., Ma, H., Carlson, B. N., Chadwick, A. J., Lamb, M. P., & Parker, G. (2019, nov). Modeling Deltaic Lobe-Building Cycles and Channel Avulsions for the Yellow River Delta, China. *Journal of Geophysical Research: Earth Surface*, *124*(11), 2438–2462. Retrieved from https://doi. doi: 10.1029/2019JF005220

Morris, B., Lawrence, A., Chilton, P., & Adams, B. (2003). *Groundwater and its susceptibility to degradation: A global assessment of the problem and options for management* (Tech. Rep.). Retrieved from http://nora.nerc.ac.uk/id/eprint/19395/

Moser, S. C., Jeffress Williams, S., & Boesch, D. F. (2012). Wicked Challenges at Land's End: Managing Coastal Vulnerability Under Climate Change. *Annual Review of Environment and Resources*, *37*(1), 51–78. Retrieved from http://www.annualreviews.org/doi/10.1146/annurev-environ-021611-135158 doi: 10.1146/annurev-environ-021611-135158

Muto, T., & Steel, R. J. (1997). Principles of regression and transgression: The nature of the interplay between accommodation and sediment supply. *Journal of Sedimentary Research, Section B: Stratigraphy and Global Studies*, *67*(6), 994–1000. doi: 10.1306/d42686a8-2b26-11d7-8648000102c1865d

Nienhuis, J. H., Ashton, A. D., Edmonds, D. A., Hoitink, A. J., Kettner, A. J., Rowland, J. C., & Törnqvist, T. E. (2020, jan). Global-scale human impact on delta morphology has led to net land area gain. *Nature*, *577*(7791), 514–518. doi: 10.1038/s41586-019-1905-9

Orton, G. J., & Reading, H. G. (1993, jun). Variability of deltaic processes in terms of sediment supply, with particular emphasis on grain size. *Sedimentology*, *40*(3), 475–512. Retrieved from `http://doi.wiley.com/10.1111/j.1365-3091.1993.tb01347.x` doi: 10.1111/j.1365-3091.1993.tb01347.x

Paola, C. (2011, jan). *In modelling, simplicity isn't simple* (Vol. 469) (No. 7328). doi: 10.1038/469038a

Pardo-Igúzquiza, E., & Dowd, P. A. (2003, jul). CONNEC3D: A computer program for connectivity analysis of 3D random set models. *Computers and Geosciences*, *29*(6), 775–785. doi: 10.1016/S0098-3004(03)00028-1

Parker, G., Muto, T., Akamatsu, Y., Dietrich, W. E., & Lauer, J. W. (2008, dec). Unravelling the conundrum of river response to rising sea-level from laboratory to field. Part I: Laboratory experiments. *Sedimentology*, *55*(6), 1643–1655. Retrieved from `http://doi.wiley.com/10.1111/j.1365-3091.2008.00961.x` doi: 10.1111/j.1365-3091.2008.00961.x

Passalacqua, P., Lanzoni, S., Paola, C., & Rinaldo, A. (2013, sep). Geomorphic signatures of deltaic processes and vegetation: The Ganges-Brahmaputra-Jamuna case study. *Journal of Geophysical Research: Earth Surface*, *118*(3), 1838–1849. Retrieved from `http://doi.wiley.com/10.1002/jgrf.20128` doi: 10.1002/jgrf.20128

Perignon, M., Adams, J., Overeem, I., & Passalacqua, P. (2020). Dominant process zones in a mixed fluvial–tidal delta are morphologically distinct. *Earth Surface Dynamics*, *8*(3), 809–824. Retrieved from `https://esurf.copernicus.org/articles/8/809/2020/` doi: 10.5194/esurf-8-809-2020

Piliouras, A., Lauzon, R., & Rowland, J. C. (2021, apr). Unraveling the Combined Effects of Ice and Permafrost on Arctic Delta Morphodynamics. *Journal of Geophysical Research: Earth Surface*, *126*(4), e2020JF005706. Retrieved from `https://onlinelibrary.wiley.com/doi/10.1029/2020JF005706` doi: 10.1029/2020jf005706

Piliouras, A., & Rowland, J. C. (2020, jan). Arctic River Delta Morphologic Variability and Implications for Riverine Fluxes to the Coast. *Journal of Geophysical Research: Earth Surface*, *125*(1), e2019JF005250. Retrieved from `https://doi.org/` doi: 10.1029/2019JF005250

Postma, G. (1995, aug). Sea-level-related architectural trends in coarse-grained delta complexes. *Sedimentary Geology*, *98*(1-4), 3–12. doi: 10.1016/0037-0738(95)00024-3

Pranter, M. J., & Sommer, N. K. (2011, jun). Static connectivity of fluvial sandstones in a lower coastal-plain setting: An example from the Upper Cretaceous lower Williams Fork Formation, Piceance Basin, Colorado. *AAPG Bulletin*, *95*(6), 899–923. Retrieved from `http://pubs.geoscienceworld.org/aapgbull/article-pdf/95/6/899/3373341/bltn10008.pdf` doi: 10.1306/12091010008

Rahman, M. M., Penny, G., Mondal, M. S., Zaman, M. H., Kryston, A., Salehin, M., … Müller, M. F. (2019, mar). *Salinization in large river deltas: Drivers, impacts and socio-hydrological feedbacks* (Vol. 6). Retrieved from `https://linkinghub.elsevier.com/retrieve/pii/S2468312418300087` doi: 10.1016/j.wasec.2019.100024

Ratliff, K. M., Hutton, E. H., & Murray, A. B. (2018, nov). Exploring Wave and Sea-Level Rise Effects on Delta Morphodynamics With a Coupled River-Ocean

Model. *Journal of Geophysical Research: Earth Surface*, *123*(11), 2887–2900. Retrieved from https://onlinelibrary.wiley.com/doi/abs/10.1029/2018JF004757 doi: 10.1029/2018JF004757

Reitz, M. D., & Jerolmack, D. J. (2012, jun). Experimental alluvial fan evolution: Channel dynamics, slope controls, and shoreline growth. *Journal of Geophysical Research: Earth Surface*, *117*(2), n/a–n/a. Retrieved from http://doi.wiley.com/10.1029/2011JF002261 doi: 10.1029/2011JF002261

Renard, P., & Allard, D. (2013, jan). Connectivity metrics for subsurface flow and transport. *Advances in Water Resources*, *51*, 168–196. Retrieved from https://www.sciencedirect.com/science/article/pii/S0309170811002223 doi: 10.1016/j.advwatres.2011.12.001

Rodriguez-Iturbe, I., Rinaldo, A., & Levy, O. (1998, jan). Fractal River Basins: Chance and Self-Organization. *Physics Today*, *51*(7), 70–71. doi: 10.1063/1.882305

Seybold, H., Andrade, J. S., & Herrmann, H. J. (2007, oct). Modeling river delta formation. *Proceedings of the National Academy of Sciences of the United States of America*, *104*(43), 16804–16809. Retrieved from http://www.ncbi.nlm.nih.gov/pubmed/17940031http://www.pubmedcentral.nih.gov/articlerender.fcgi?artid=PMC2040410 doi: 10.1073/pnas.0705265104

Shamsudduha, M., Taylor, R. G., Ahmed, K. M., & Zahid, A. (2011, jun). The impact of intensive groundwater abstraction on recharge to a shallow regional aquifer system: Evidence from Bangladesh. *Hydrogeology Journal*, *19*(4), 901–916. Retrieved from https://ui.adsabs.harvard.edu/abs/2011HydJ...19..901S/abstract doi: 10.1007/s10040-011-0723-4

Shaw, J. B., & Mohrig, D. (2014, jan). The importance of erosion in distributary channel network growth, Wax Lake Delta, Louisiana, USA. *Geology*, *42*(1), 31–34. Retrieved from https://pubs.geoscienceworld.org/geology/article/42/1/31-34/131325 doi: 10.1130/G34751.1

Shaw, J. B., Mohrig, D., & Whitman, S. K. (2013, sep). The morphology and evolution of channels on the Wax Lake Delta, Louisiana, USA. *Journal of Geophysical Research: Earth Surface*, *118*(3), 1562–1584. Retrieved from http://doi.wiley.com/10.1002/jgrf.20123 doi: 10.1002/jgrf.20123

Shaw, J. B., Wolinsky, M. A., Paola, C., & Voller, V. R. (2008, jun). An image-based method for shoreline mapping on complex coasts. *Geophysical Research Letters*, *35*(12), n/a–n/a. Retrieved from http://doi.wiley.com/10.1029/2008GL033963 doi: 10.1029/2008GL033963

Stocker, T. F., Qin, D., Plattner, G.-K., Tignor, M., Allen, S. K., Boschung, J., … others (2013). Climate change 2013. the physical science basis. working group i contribution to the fifth assessment report of the intergovernmental panel on climate change-abstract for decision-makers; changements climatiques 2013. les elements scientifiques. contribution du groupe de travail i au cinquieme rapport d'evaluation du groupe d'experts intergouvernemental sur l'evolution du climat-resume a l'intention des decideurs.

Straub, K. M., Li, Q., & Benson, W. M. (2015, nov). Influence of sediment cohesion on deltaic shoreline dynamics and bulk sediment retention: A laboratory study. *Geophysical Research Letters*, *42*(22), 9808–9815. Retrieved from http://doi.wiley.com/10.1002/2015GL066131 doi: 10.1002/2015GL066131

Strong, N., Sheets, B. A., Hickson, T. A., & Paola, C. (2005). A mass-balance framework for quantifying downstream changes in fluvial architecture. In *Fluvial sedimentology vii* (Vol. 35, pp. 243–253). International Association of Sedimentologists Special Publication 35.

Syvitski, J. P., Kettner, A. J., Overeem, I., Hutton, E. W., Hannon, M. T., Brakenridge, G. R., … Nicholls, R. J. (2009, oct). Sinking deltas due to human activities. *Nature Geoscience*, *2*(10), 681–686. Retrieved from

http://www.nature.com/articles/ngeo629 doi: 10.1038/ngeo629
Syvitski, J. P., & Saito, Y. (2007, jun). Morphodynamics of deltas under the influence of humans. *Global and Planetary Change*, *57*(3-4), 261–282. Retrieved from https://www.sciencedirect.com/science/article/pii/S0921818106003146 doi: 10.1016/j.gloplacha.2006.12.001
Tanabe, S., Ta, T. K. O., Nguyen, V. L., Tateishi, M., Kobayashi, I., & Saito, Y. (2003). Delta Evolution Model Inferred From the Holocene Mekong Delta, Southern Vietnam. In *Tropical deltas of southeast asia* (Vol. 76, pp. 175–188). Special Publications of SEPM. doi: 10.2110/pec.03.76.0175
Toby, S. C., Duller, R. A., De Angelis, S., & Straub, K. M. (2019, may). A Stratigraphic Framework for the Preservation and Shredding of Environmental Signals. *Geophysical Research Letters*, *46*(11), 5837–5845. Retrieved from https://onlinelibrary.wiley.com/doi/abs/10.1029/2019GL082555 doi: 10.1029/2019GL082555
Twilley, R. R., Bentley, S. J., Chen, Q., Edmonds, D. A., Hagen, S. C., Lam, N. S., ... McCall, A. (2016). Co-evolution of wetland landscapes, flooding, and human settlement in the Mississippi River Delta Plain. *Sustainability Science*, *11*(4), 711–731. doi: 10.1007/s11625-016-0374-4
Tye, R. S., & Coleman, J. M. (1989). Depositional processes and stratigraphy of fluvially dominated lacustrine deltas: Mississippi delta plain. *Journal of Sedimentary Petrology*, *59*(6), 973–996. doi: 10.1306/212F90CA-2B24-11D7-8648000102C1865D
Van de Lageweg, W. I., van Dijk, W. M., & Kleinhans, M. G. (2013, apr). Channel belt architecture formed by a meandering river. *Sedimentology*, *60*(3), 840–859. Retrieved from http://doi.wiley.com/10.1111/j.1365-3091.2012.01365.x doi: 10.1111/j.1365-3091.2012.01365.x
Winkel, L., Berg, M., Amini, M., Hug, S. J., & Johnson, A. A. (2008, aug). Predicting groundwater arsenic contamination in Southeast Asia from surface parameters. *Nature Geoscience*, *1*(8), 536–542. Retrieved from http://www.nature.com/articles/ngeo254 doi: 10.1038/ngeo254
Wolinsky, M. A., Edmonds, D. A., Martin, J., & Paola, C. (2010, nov). Delta allometry: Growth laws for river deltas. *Geophysical Research Letters*, *37*(21), n/a–n/a. Retrieved from http://doi.wiley.com/10.1029/2010GL044592 doi: 10.1029/2010GL044592
Xu, Z., Hariharan, J., Passalacqua, P., Steel, E., Paola, C., & Michael, H. A. (accepted). Constraining subsurface properties from surface information in river deltas – part 2: Relating subsurface geometries and groundwater behavior. *Submitted to Water Resources Research*.
Yang, N., Winkel, L. H., & Johannesson, K. H. (2014, may). Predicting geogenic arsenic contamination in shallow groundwater of South Louisiana, United States. *Environmental Science and Technology*, *48*(10), 5660–5666. Retrieved from http://pubs.acs.org/doi/10.1021/es405670g doi: 10.1021/es405670g

## References From the Supporting Information

Garcia, M., & Parker, G. (1991, apr). Entrainment of Bed Sediment into Suspension. *Journal of Hydraulic Engineering*, *117*(4), 414–435. Retrieved from https://ascelibrary.org/doi/abs/10.1061/%28ASCE%290733-9429%281991%29117%3A4%28414%29 doi: 10.1061/(asce)0733-9429(1991)117:4(414)
Liang, M., Geleynse, N., Edmonds, D. A., & Passalacqua, P. (2015). A reduced-complexity model for river delta formation - Part 2: Assessment of the flow routing scheme. *Earth Surface Dynamics*, *3*(1), 87–104. Retrieved from www.earth-surf-dynam.net/3/87/2015/ doi: 10.5194/esurf-3-87-2015
Liang, M., Voller, V. R., & Paola, C. (2015). A reduced-complexity model for river delta formation - Part 1: Modeling deltas with channel dynamics. *Earth Sur-*

*face Dynamics*, *3*(1), 67–86. Retrieved from www.earth-surf-dynam.net/3/67/2015/ doi: 10.5194/esurf-3-67-2015

Mahmud, K., Mariethoz, G., Caers, J., Tahmasebi, P., & Baker, A. (2014, apr). Simulation of Earth textures by conditional image quilting. *Water Resources Research*, *50*(4), 3088–3107. Retrieved from http://doi.wiley.com/10.1002/2013WR015069 doi: 10.1002/2013WR015069

Meyer-Peter, E., & Müller, R. (1948). Formulas for Bed-Load transport. *IAHSR 2nd meeting, Stockholm, appendix 2*. Retrieved from https://repository.tudelft.nl/islandora/object/uuid%3A4fda9b61-be28-4703-ab06-43cdc2a21bd7

van Rijn, L. C. (1984, nov). Sediment Transport, Part II: Suspended Load Transport. *Journal of Hydraulic Engineering*, *110*(11), 1613–1641. Retrieved from https://ascelibrary.org/doi/abs/10.1061/%28ASCE%290733-9429%281984%29110%3A11%281613%29 doi: 10.1061/(asce)0733-9429(1984)110:11(1613)

Virtanen, P., Gommers, R., Oliphant, T. E., Haberland, M., Reddy, T., Cournapeau, D., . . . SciPy 1.0 Contributors (2020). SciPy 1.0: Fundamental Algorithms for Scientific Computing in Python. *Nature Methods*, *17*, 261–272. doi: 10.1038/s41592-019-0686-2

Xu, Z., Hariharan, J., Passalacqua, P., Steel, E., Paola, C., & Michael, H. A. (accepted). Constraining subsurface properties from surface information in river deltas – part 2: Relating subsurface geometries and groundwater behavior. *Submitted to Water Resources Research*.

**Figure 1.**

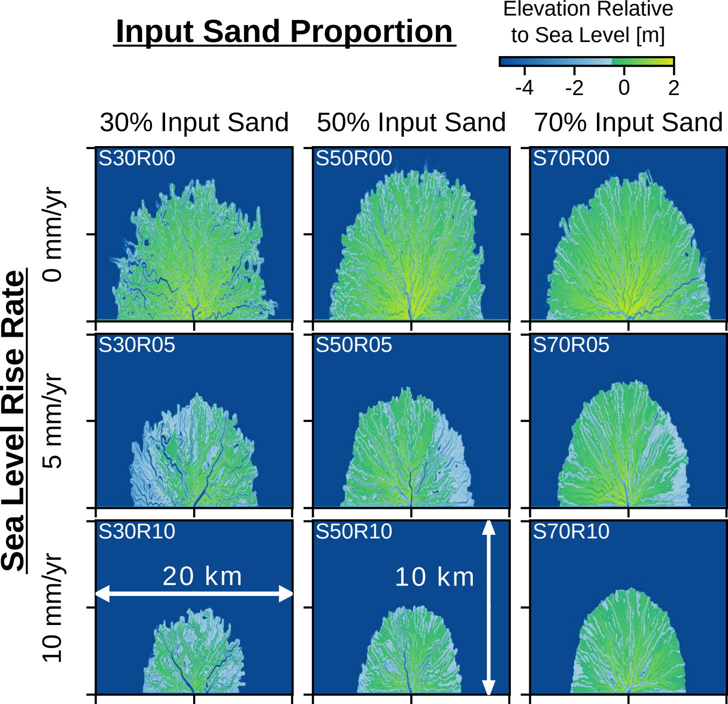

Input Sand Proportion
Elevation Relative to Sea Level [m]
-4
-2
0
2
30% Input Sand
50% Input Sand
70% Input Sand
Sea Level Rise Rate
0 mm/yr
5 mm/yr
10 mm/yr
S30R00
S50R00
S70R00
S30R05
S50R05
S70R05
S30R10
S50R10
S70R10
20 km
10 km

**Figure 2.**

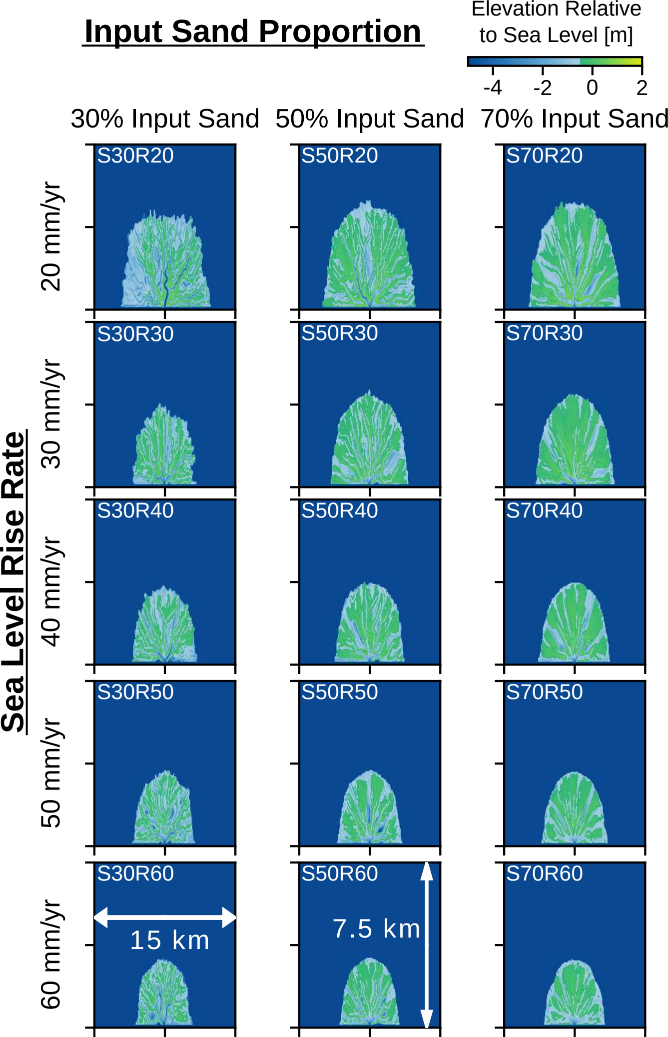

Input Sand Proportion
Elevation Relative to Sea Level [m]
-4
-2
0
2
30% Input Sand
50% Input Sand
70% Input Sand
Sea Level Rise Rate
20 mm/yr
30 mm/yr
40 mm/yr
50 mm/yr
60 mm/yr
S30R20
S50R20
S70R20
S30R30
S50R30
S70R30
S30R40
S50R40
S70R40
S30R50
S50R50
S70R50
S30R60
S50R60
S70R60
15 km
7.5 km

**Figure 3.**

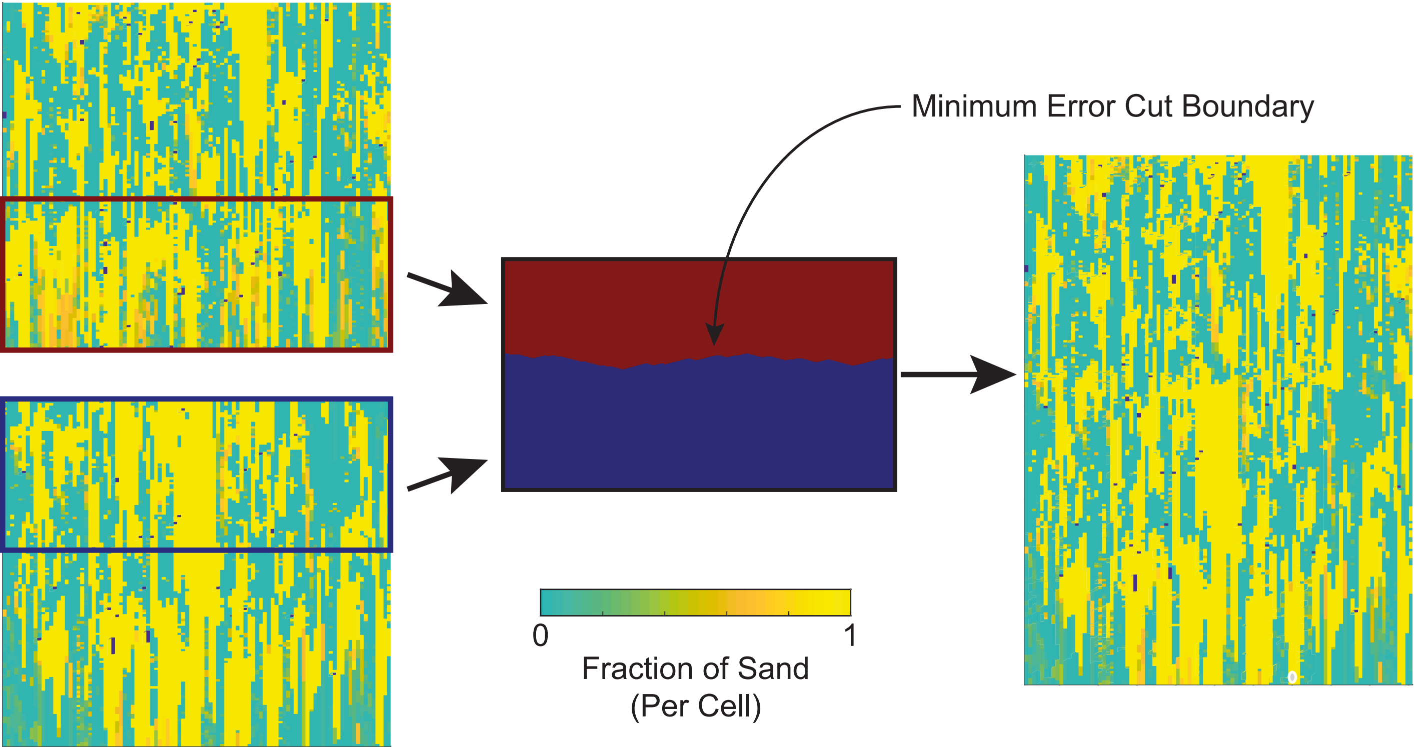
Minimum Error Cut Boundary
0
1
Fraction of Sand
(Per Cell)

**Figure 4.**

30%
A'
50%
A
10%
0
Fraction of Sand
(Per Cell)
1
(a)
5m
A
A'
10%
30%
7.5m
(b)

**Figure 5.**

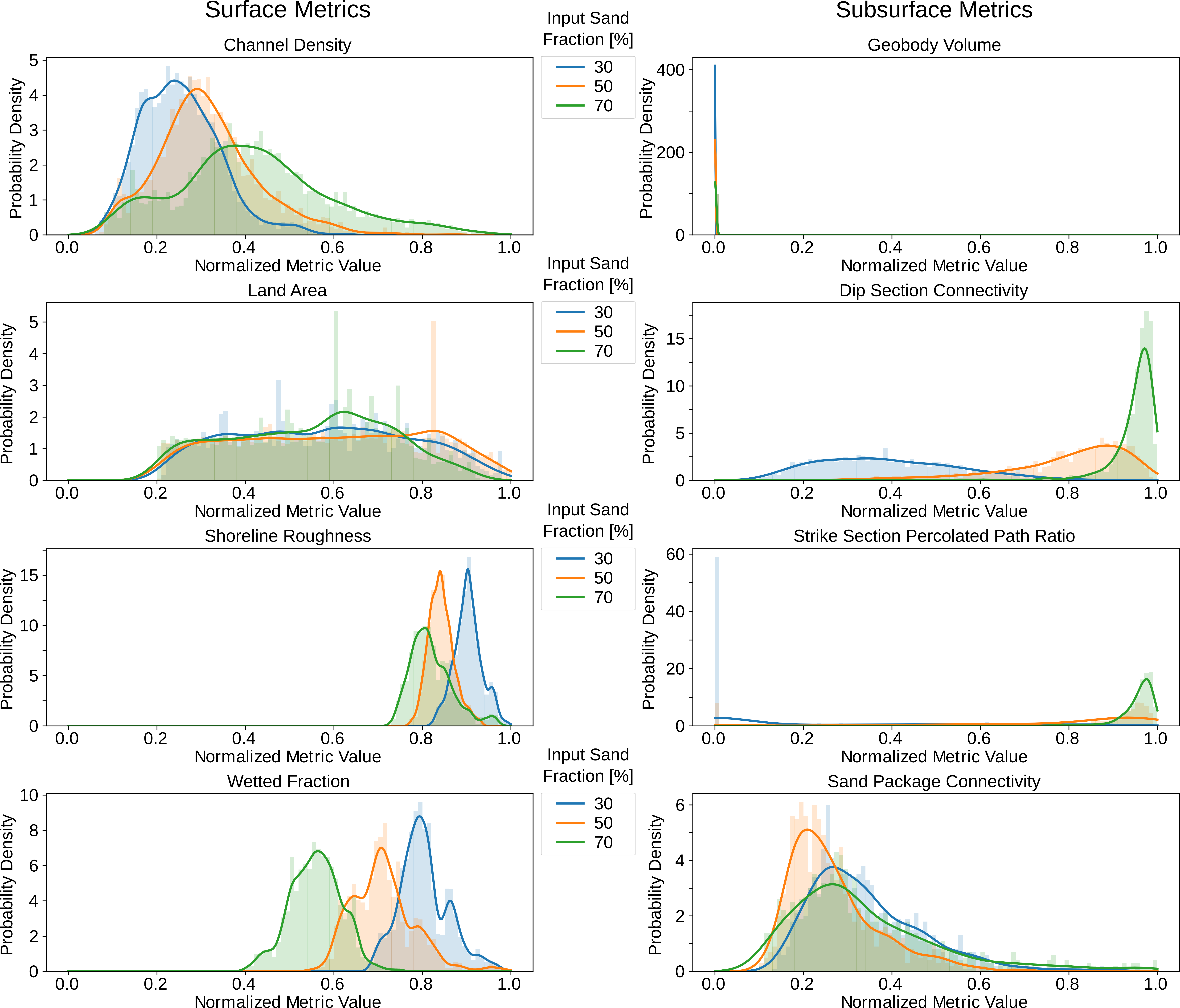

Surface Metrics
Subsurface Metrics
Channel Density
Land Area
Shoreline Roughness
Wetted Fraction
Geobody Volume
Dip Section Connectivity
Strike Section Percolated Path Ratio
Sand Package Connectivity
Input Sand Fraction [%]
30
50
70
Probability Density
Normalized Metric Value

**Figure 6.**

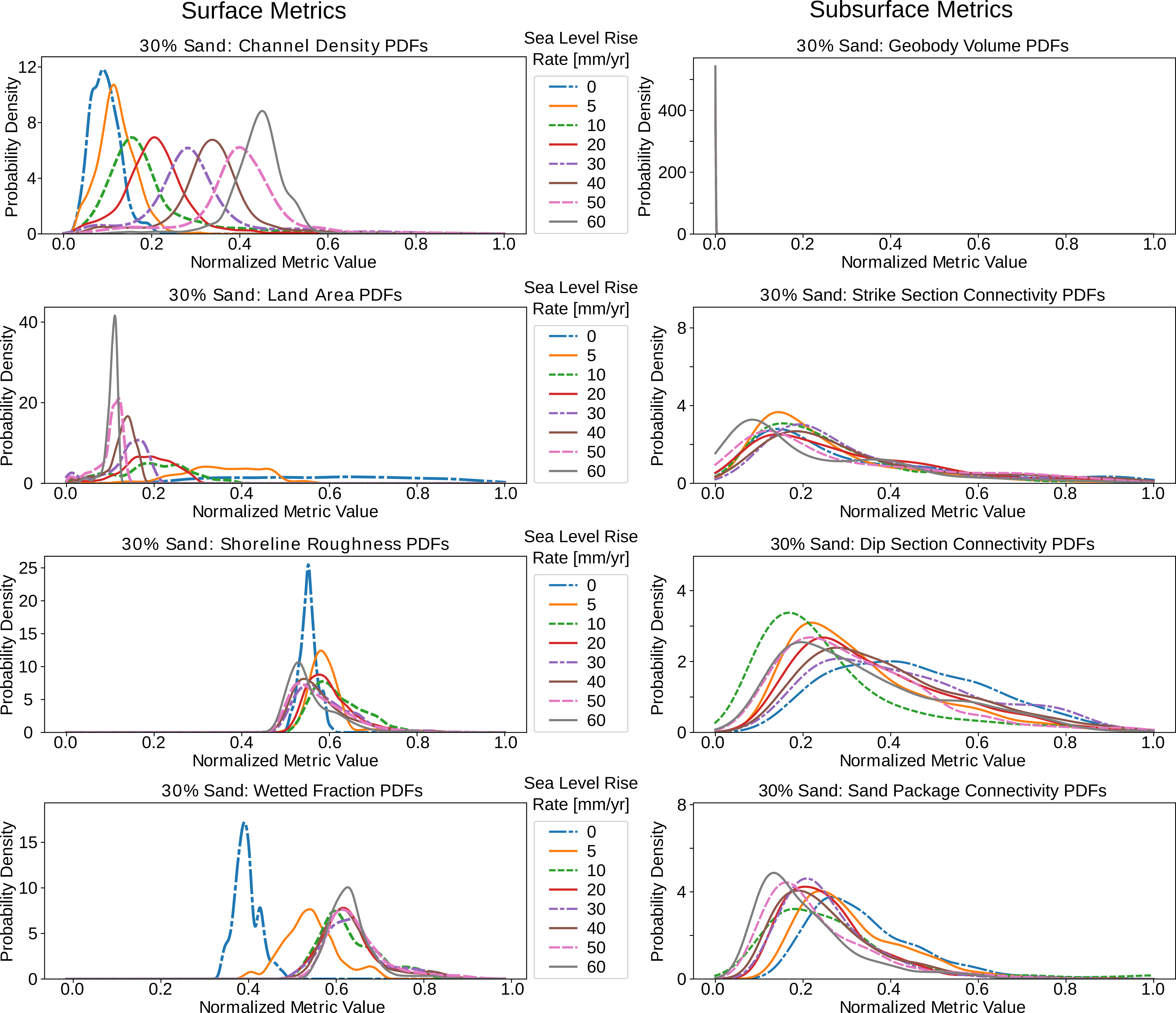
Surface Metrics
Subsurface Metrics
30% Sand: Channel Density PDFs
30% Sand: Geobody Volume PDFs
30% Sand: Land Area PDFs
30% Sand: Strike Section Connectivity PDFs
30% Sand: Shoreline Roughness PDFs
30% Sand: Dip Section Connectivity PDFs
30% Sand: Wetted Fraction PDFs
30% Sand: Sand Package Connectivity PDFs
Sea Level Rise Rate [mm/yr]
0
5
10
20
30
40
50
60
Probability Density
Normalized Metric Value

**Figure 7.**

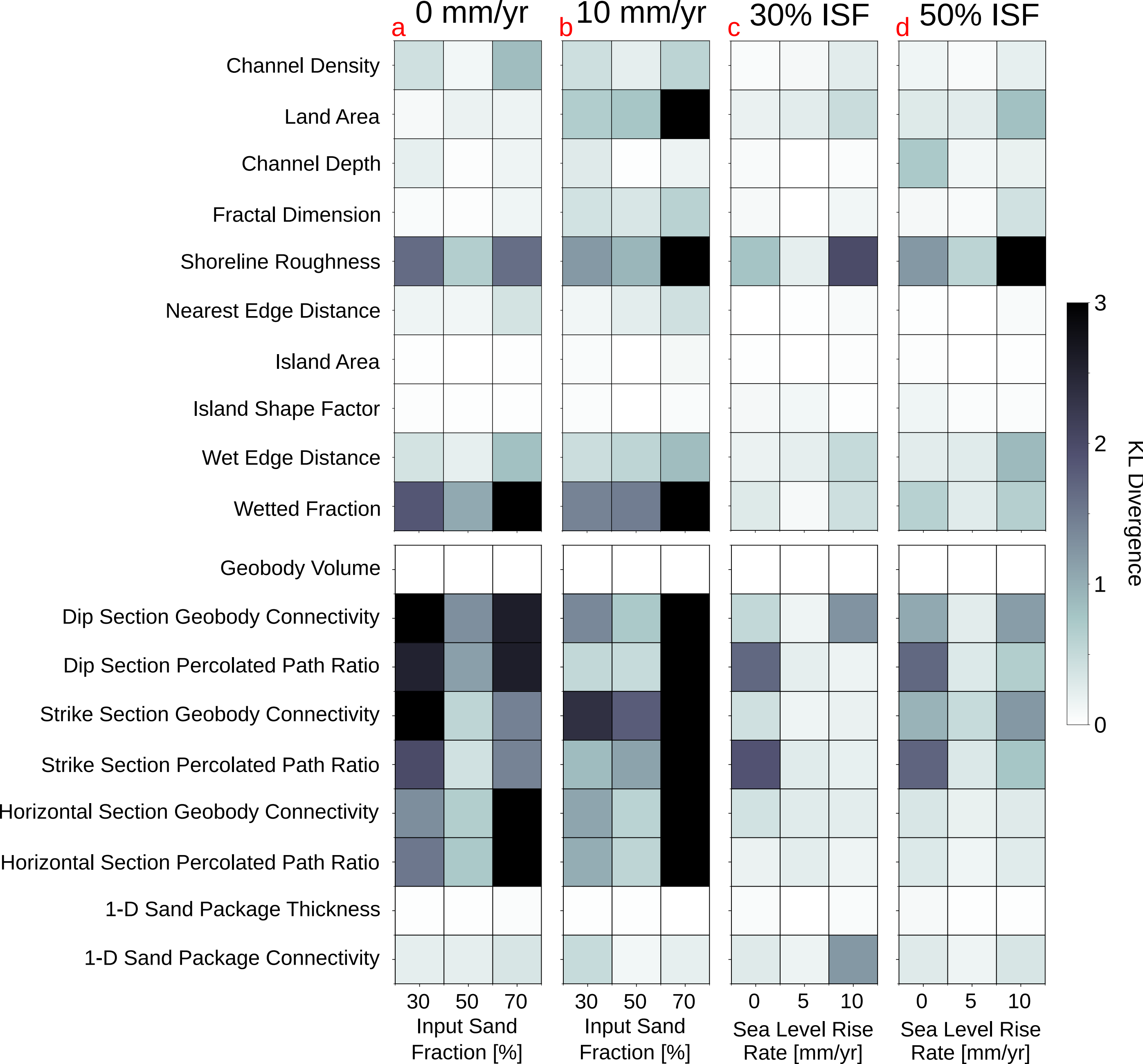

a 0 mm/yr
b 10 mm/yr
c 30% ISF
d 50% ISF
Channel Density
Land Area
Channel Depth
Fractal Dimension
Shoreline Roughness
Nearest Edge Distance
Island Area
Island Shape Factor
Wet Edge Distance
Wetted Fraction
Geobody Volume
Dip Section Geobody Connectivity
Dip Section Percolated Path Ratio
Strike Section Geobody Connectivity
Strike Section Percolated Path Ratio
Horizontal Section Geobody Connectivity
Horizontal Section Percolated Path Ratio
1-D Sand Package Thickness
1-D Sand Package Connectivity
30 50 70
Input Sand Fraction [%]
0 5 10
Sea Level Rise Rate [mm/yr]
KL Divergence
0 1 2 3

**Figure 8.**

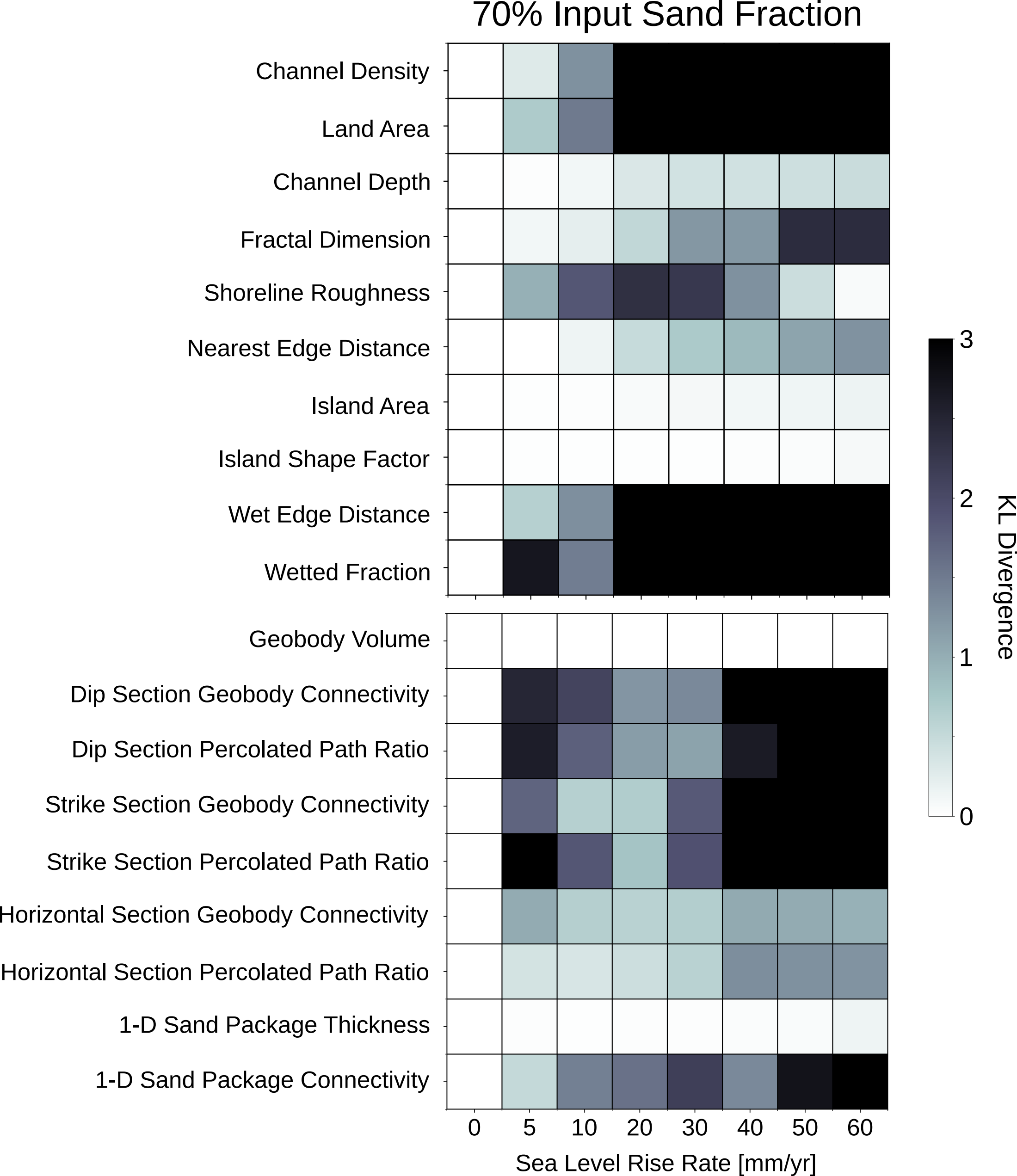
70% Input Sand Fraction
Channel Density
Land Area
Channel Depth
Fractal Dimension
Shoreline Roughness
Nearest Edge Distance
Island Area
Island Shape Factor
Wet Edge Distance
Wetted Fraction
Geobody Volume
Dip Section Geobody Connectivity
Dip Section Percolated Path Ratio
Strike Section Geobody Connectivity
Strike Section Percolated Path Ratio
Horizontal Section Geobody Connectivity
Horizontal Section Percolated Path Ratio
1-D Sand Package Thickness
1-D Sand Package Connectivity
0
5
10
20
30
40
50
60
Sea Level Rise Rate [mm/yr]
KL Divergence
0
1
2
3